JOURNAL OF PETROLOGY

Journal of Petrology, 2015, Vol. 56, No. 6, 1173–1197
doi: 10.1093/petrology/egv033
Original Article

OXFORD

Petrology and Geochemistry of Volcanic Rocks from the South Kaua`i Swell Volcano, Hawai`i: Implications for the Lithology and Composition of the Hawaiian Mantle Plume

Michael O. Garcia[1]*, Dominique Weis[2], Lisa Swinnard[1†], Garrett Ito[1] and Aaron J. Pietruszka[3]

[1]Department of Geology and Geophysics, University of Hawai`i, Honolulu, HI 96822, USA, [2]Department of Earth and Ocean Sciences, University of British Columbia, Vancouver, BC, V6T 1Z4, Canada and [3]US Geological Survey, Denver Federal Center, Denver, CO 80225, USA

*Corresponding author. Telephone: (1) 808 956 6641. Fax: (1) 808 956 5512. E-mail: mogarcia@hawaii.edu
[†]Present address: ARANZ Geo Canada Ltd, 506–1168 Hamilton Street, Vancouver, BC, V6B 2S2, Canada.

Received November 1, 2014; Accepted June 1, 2015

ABSTRACT

The South Kaua`i Swell (SKS) volcano was sampled during four JASON dives and three dredge hauls recovering rocks that range from fresh pillow lavas to altered volcanic breccias. Two geochemical groups were identified: shield-stage tholeiites (5·4–3·9 Ma) and rejuvenation-stage alkalic lavas (1·9–0·1 Ma). The young SKS ages and the coeval rejuvenated volcanism along a 400 km segment of the Hawaiian Islands (Maui to Ni`ihau) are inconsistent with the timing and duration predictions by the flexure and secondary plume melting models for renewed volcanism. The SKS tholeiites are geochemically heterogeneous but similar to lavas from nearby Kaua`i, Ni`ihau and Wai`anae volcanoes, indicating that their source regions within the Hawaiian mantle plume sampled a well-mixed zone. Most SKS tholeiitic lavas exhibit radiogenic Pb isotope ratios ($^{208}Pb^*/^{206}Pb^*$) that are characteristic of Loa compositions (>0·9475), consistent with the volcano's location on the west side of the Hawaiian Islands. These results document the existence of the Loa component within the Hawaiian mantle plume prior to 5 Ma. Loa trend volcanoes are thought to have a major pyroxenite component in their source. Calculations of the pyroxenitic component in the parental melts for SKS tholeiites using high-precision olivine analyses and modeling of trace element ratios indicate a large pyroxenite proportion (≥50%), which was predicted by recent numerical models. Rejuvenation-stage lavas were also found to have a significant pyroxenite component based on olivine analyses (40–60%). The abundance of pyroxenite in the source for SKS lavas may be the cause of this volcano's extended period of magmatism (>5 Myr). The broad distribution of the Loa component in the northern Hawaiian Island lavas coincides with the start of a dramatic magma flux increase (300%) along the Hawaiian Chain, which may reflect a major structural change in the source of the Hawaiian mantle plume.

Key words: Hawaii; basalt; geochemistry; submarine volcano; mantle plume heterogeneities

INTRODUCTION

Volcanoes of widely varying size, shape and origin occur on the seafloor around the main Hawaiian Islands (e.g. Holcomb & Robinson, 2004). Some are satellite vents formed coevally with the giant shield volcanoes (e.g. Mauna Loa; Wanless *et al.*, 2006), most are related to rejuvenated or secondary volcanism (e.g. around the islands of Ni`ihau and Ka`ula; Clague *et al.*, 2000; Garcia

et al., 2008), and a few are broad submarine shields with low aspect ratios (slopes of <1·5°) (e.g. Southwest O'ahu volcano, Takahashi *et al.*, 2001; Coombs *et al.*, 2004; South Kauai Swell volcano, Ito *et al.*, 2013; Fig. 1). The South Kauai Swell volcano (SKS) contains numerous (>50), small (100–1100 m wide), cone-shaped seamounts on a broad convex surface that meets the surrounding abyssal seafloor with a distinct slope break (Fig. 1). The volume of SKS [$(\sim 14 \pm 3{\cdot}4) \times 10^3$ km^3; Ito *et al.*, 2013] is equivalent to a medium-size Hawaiian shield volcano (e.g. Hualālai; Robinson & Eakins, 2006).

Volcanic rock samples (111) were collected from SKS at 20 seamounts and five other areas at depths of 3–4 km below sea level (Fig. 2) using the University of Hawai`i R.V. *Kilo Moana*. Most samples (96) were collected using the JASON ROV on dives 252, 297, 298 and 299 [for maps showing dive locations, see supplementary materials of Ito *et al.* (2013)]. Field observations via the JASON video camera indicate that most samples were collected in place. Fifteen volcanic rocks were also recovered from dredge hauls KS1, 2 and 3 (Fig. 2). Maps for the three dredge haul locations are provided in Supplementary Data Electronic Appendix 1 (available for downloading at http://www.petrology.oxfordjournals.org).

Here we present new petrology and geochemistry results for samples from SKS. The goals of this work were to characterize the volcanic rocks from this previously unknown shield volcano, use these results to evaluate its origin and to compare the geochemistry of SKS lavas with results for lavas from other northern Hawaiian Island volcanoes (west to east and older to younger; Ni`ihau, Kaua`i, West Ka`ena and Wai`anae). Petrography and mineral chemistry are presented to characterize the magmatic history and source lithology of SKS lavas. Whole-rock X-ray fluorescence (XRF) major and trace element and inductively coupled plasma mass spectrometry (ICP-MS) trace element data are used to characterize the SKS rock types and their magmatic evolution. Isotopes of Pb, Sr, Nd and Hf are presented to characterize the source for SKS lavas (Kea vs Loa type chemistry; e.g. Weis *et al.*, 2011; Jackson *et al.*, 2012) and to compare it with the source for adjacent volcanoes. Estimates of the amount of pyroxenite component in melts from the SKS source are given based on olivine chemistry and trace element modeling

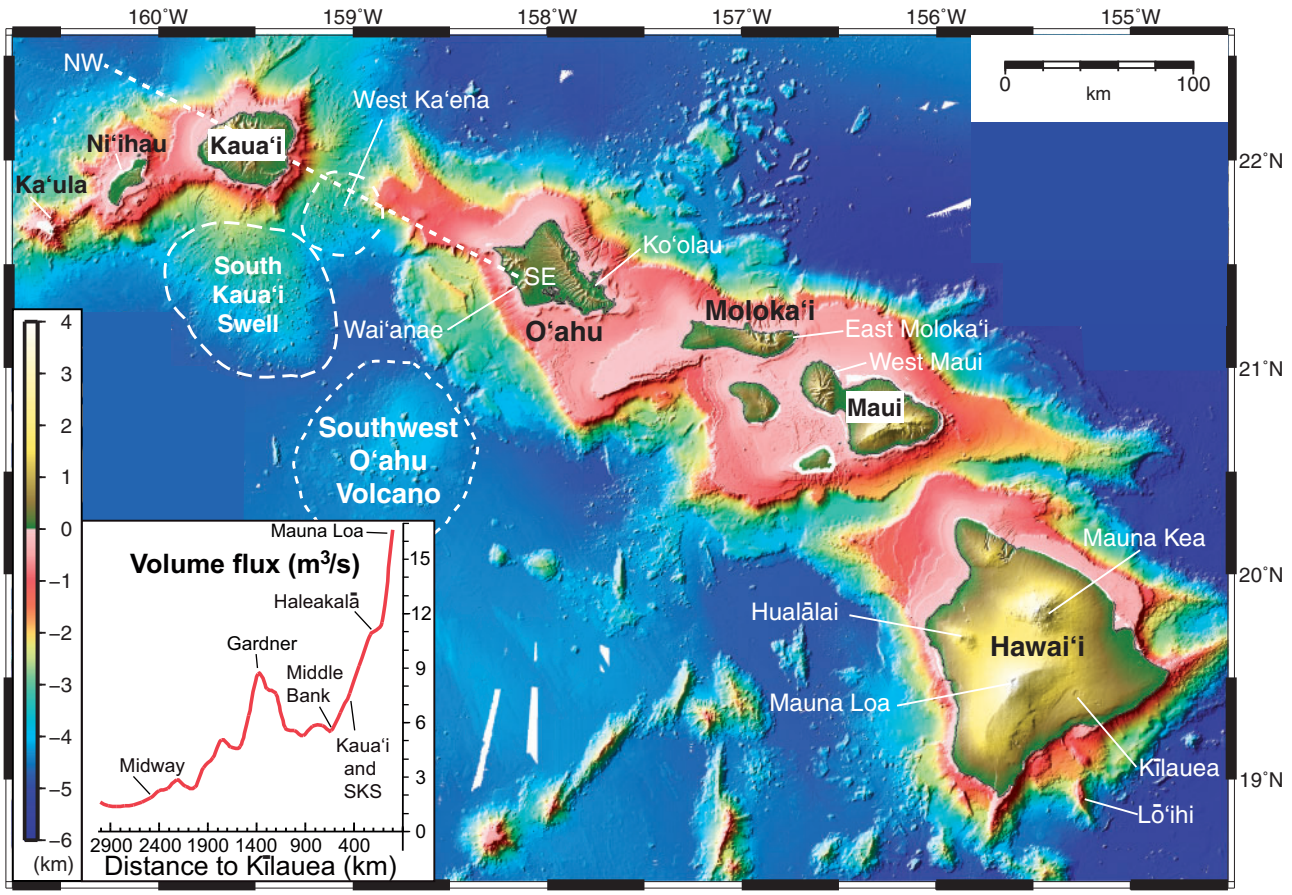

Fig. 1. Multibeam bathymetry map of the Hawaiian Islands, illuminated from the NW (grid available at http://www.soest.hawaii.edu/HMRG/cms). The boundaries of the Hawaiian low-aspect ratio volcanoes, SW Oahu and South Kauai Swell, are shown by white dashed lines. The line labeled NW–SE shows the location of the section in Fig. 13. Inset: temporal variation in magma flux (m^3 s^{-1}) for the Hawaiian Ridge (red line) estimated using a flexural compensation model (modified after Vidal & Bonneville, 2004). The nearly 300% increase in magma flux for the Hawaiian Islands (just after Middle Bank to Mauna Loa, at the young end of the Ridge) should be noted.

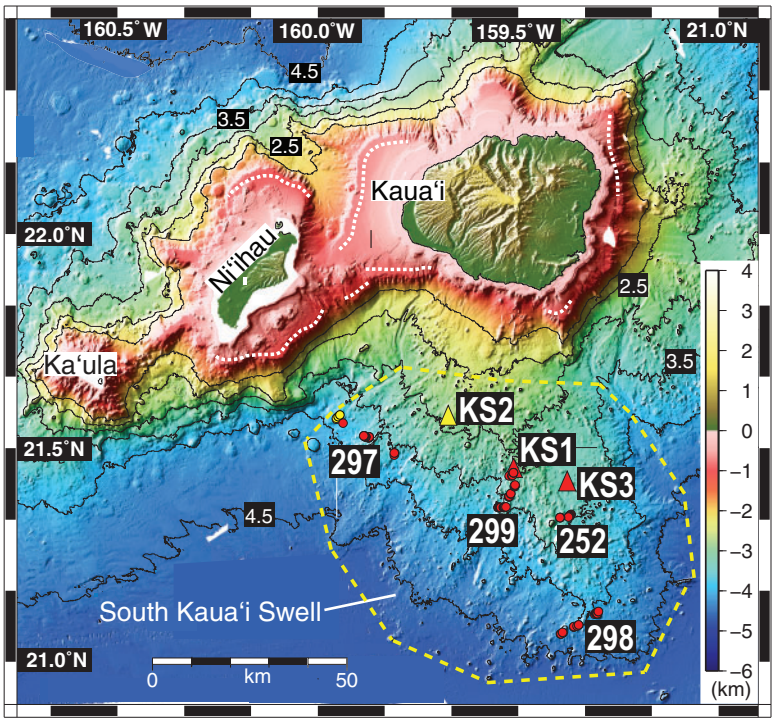

Fig. 2. Shaded relief map of the South Kaua`i Swell volcano (enclosed by dashed yellow line) and the islands of Kaua`i, Ni`ihau and Ka`ula. Locations where SKS samples were collected during JASON dives 252, 297, 298 and 299 are shown by red circles (dive numbers are indicated). Locations of dredge hauls (KS1, 2 and 3) are shown by triangles. Red circles and triangles are for tholeiitic rocks; yellow symbols are for alkalic samples. The white dotted lines around parts of the islands of Ni`ihau and Kaua`i mark the former maximum shoreline for these islands during the shield stage of growth (Flinders *et al.*, 2010). The gap in the old Kaua`i shoreline on the south side of island is thought to have been produced by a landslide (Ito *et al.*, 2013). Bathymetry contours are in 500 m intervals starting at 2 km.

using the methods of Gurenko *et al.* (2010) and Pietruszka *et al.* (2013). These results are compared with those inferred from dynamic modeling of the interaction of small-scale convection rolls with the Hawaiian plume (Ballmer *et al.*, 2011). A comparison is made of radiometric ages of SKS with those for lavas from adjacent volcanoes to examine the temporal evolution of shield growth for the northern Hawaiian Islands, and to evaluate models for the origin of Hawaiian rejuvenation volcanism.

SAMPLES

The SKS volcanic samples range from pillow lavas (75% of the sample suite) to volcanic breccias (25%). Sample collection locations and basic hand specimen features (weight, size, presence and thickness of glass and manganese coating, and extent of alteration) for the SKS volcanic rocks are given in Supplementary Data Electronic Appendix 2. Most of the SKS breccias consist of lithologically identical, angular clasts (monomict). Monomict breccias were found in the drill core from the second phase of the Hawaii Scientific Drilling Project (HSDP2), which was located on the flanks of dormant Mauna Kea volcano on the Island of Hawai`i. These breccias were interpreted to have formed as lavas erupted on Mauna Kea's submarine slopes (Garcia *et al.*, 2007). We propose the SKS lavas to have a similar origin. Only the SKS monolithic breccias and pillow lavas are discussed below.

Radiometric ages for SKS samples were reported by Ito *et al.* (2013). These include 15 ages by $^{40}Ar/^{39}Ar$ and nine using the unspiked K–Ar method (see Supplementary Data Electronic Appendix 2). All of the alkalic samples and the one transitional sample were analyzed by the unspiked K–Ar method, yielding ages of 0·1–1·9 Ma. Two older, tholeiitic SKS samples were analyzed with both the unspiked K–Ar and $^{40}Ar/^{39}Ar$ methods. These samples yielded remarkably consistent ages by the two methods: $4{\cdot}24 \pm 0{\cdot}46$ Ma by K–Ar vs $4{\cdot}14 \pm 0{\cdot}14$ Ma and $4{\cdot}22 \pm 0{\cdot}12$ Ma by $^{40}Ar/^{39}Ar$ for sample 297–09 (all errors are 2σ), and $4{\cdot}03 \pm 0{\cdot}12$ Ma by K–Ar and $4{\cdot}02 \pm 0{\cdot}13$ Ma by $^{40}Ar/^{39}Ar$ for sample 299–29 (Ito *et al.*, 2013). The SKS ages span an unusually large time range (0·1–5·4 Ma) for a single Hawaiian volcano. The tholeiitic samples are distinctly older (3·9–5·4 Ma) than the alkalic and the transitional lavas (0·1–1·9 Ma). The apparent 2·0 Myr gap in volcanism is comparable with the gap observed between shield and rejuvenated lava sequences on neighboring Ni`ihau volcano (Sherrod *et al.*, 2007*b*).

Petrography

The SKS rocks show varying degrees of alteration from unaltered (fresh glass with pristine olivine and open vesicles; Fig. 3) to moderate alteration with partial

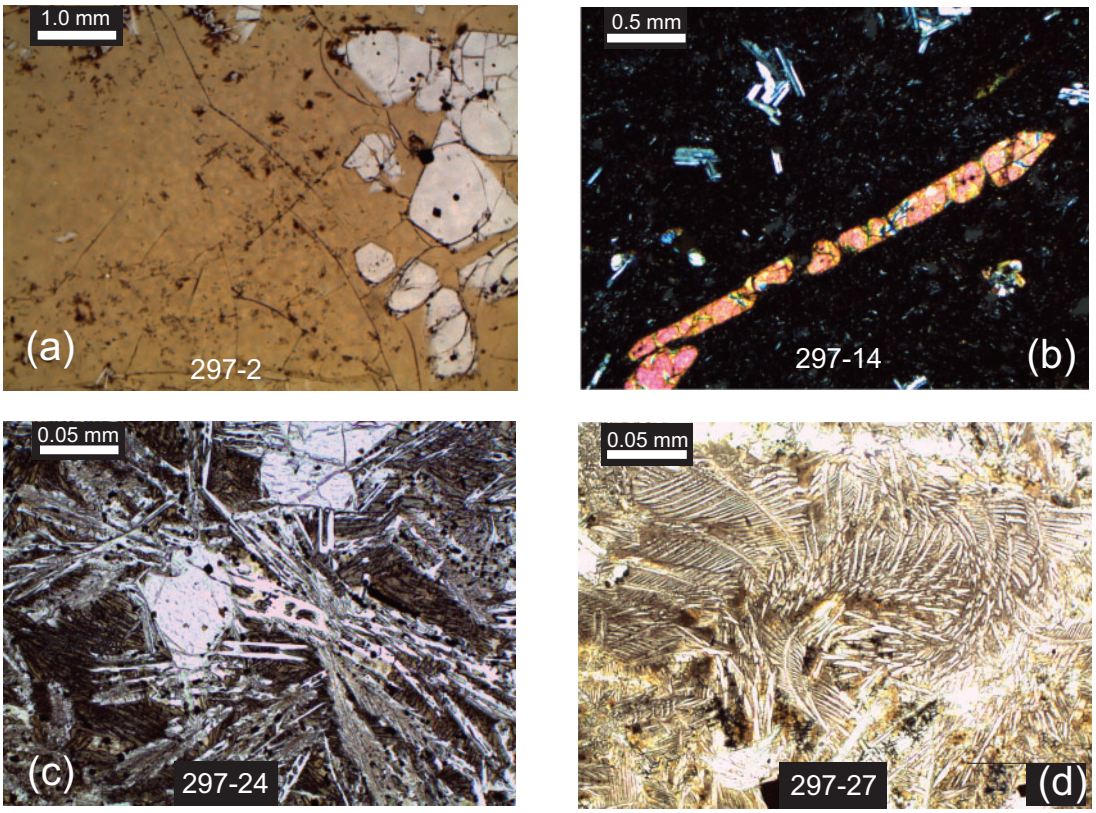

Fig. 3. Photomicrographs of SKS lavas showing rapid quenching textures. Sample numbers are given at the base and a scale bar at the top left on each image. (a) Plane-polarized light image of brown glassy matrix with olivine crystals from tholeiitic sample 297-2. (b) Cross-polarized light image of strongly elongate olivine in a glassy matrix from tholeiitic sample 297-14. (c) Cross-polarized light image showing small euhedral olivine and crystals with hopper and dendritic morphologies in transitional basalt 297-24. (d) Plain-polarized light image of feathery clinopyroxene crystals in tholeiitic lava 297-27.

replacement of olivine by iddingsite and clay and/or zeolite coatings of vesicles. Generally, there is a direct correlation of alteration level and vesicularity, which is highly variable in SKS tholeiitic lavas (<0·1–46 vol. % vesicles; Fig. 4) with a mean value of 13 vol. %. Most samples (56%) contain <5·4 vol. % vesicles; however, many (32%) are strongly vesicular (>20 vol. %) and some (12%) are moderately vesicular (10–18 vol. %; Table 1). All six of the alkalic lavas and the one transitional lava are weakly vesicular (Table 1; Fig. 4). There is no systematic variation in vesicularity with sampling location, although samples from dive 298, which were collected at depths of 3570–4160 m below sea level and furthest from the island of Kaua`i (Fig. 1), are all weakly vesicular (Table 1). The highly vesicular SKS samples were collected from the western (dive 297, water depths 3330–3770 m) and central parts (dives 252 and 299, water depths 3260–3322 m) of the SKS (Fig. 2). However, some of the cones with multiple samples have both strongly and weakly vesicular samples (dive 297, cones B and E; dive 252, cone B), whereas other cones have only strongly vesicular samples (dive 297, cone C) or only weakly vesicular samples (dive 297, cone D; dive 298, cone D). The weakly vesicular tholeiitic lavas span a wide age range (3·9–5·4 Ma) and include all four of the older samples (>4·7 Ma).

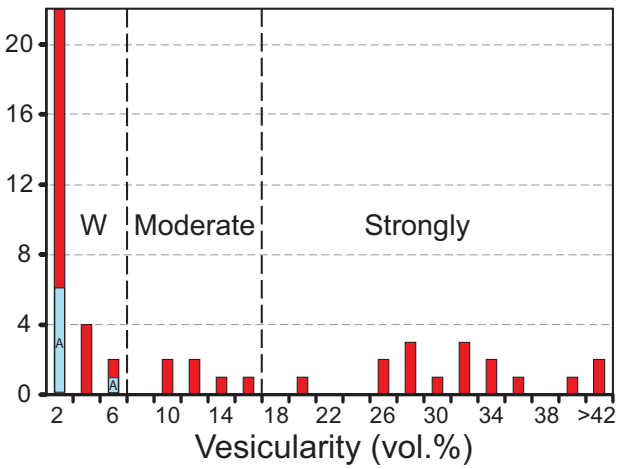

Fig. 4. Histogram of vesicularity (vol. %) in SKS lavas. Tholeiitic lavas are shown in red and alkalic lavas in blue with an 'A' symbol. Most SKS lavas are weakly vesicular (W, <8 vol. %), some are moderately vesicular (10–18 vol. %) and many are strongly vesicular (>20 vol. %). Vesicularity based on 300 counts per sample (data from Table 1).

The groundmass texture of the SKS lavas is highly variable. Some samples are glassy with dendritic plagioclase microlites (Fig. 3), which is indicative of rapid quenching (e.g. Lofgren, 1974) such as in a

Table 1: Petrography of SKS lavas (500 points, vesicle-free; vol. %)

Sample	Olivine			Plag	Cpx	Ground	Vesicles
no.	ph	mph	xeno	mph	mph	-mass	
Tholeiite							
252-02	6·2	3·8	0·0	0·0	0·0	90·0	30·8
252-04	1·0	0·2	0·0	0·4	0·0	98·4	0·6
252-05	10·4	5·4	0·0	0·6	1·4	82·2	13·2
252-07	3·0	2·6	1·4	0·2	0·0	92·8	24·4
252-09	2·2	0·4	0·0	1·2	0·8	95·4	32·8
252-10	1·4	0·8	0·0	0·0	0·0	97·8	26·2
297-01	3·3	4·7	1·7	0·0	0·3	90·0	11·0
297-02	0·0	1·7	0·0	0·3	0·0	98·0	3·0
297-04	5·3	3·3	1·4	3·0	0·0	87·0	29·0
297-05	4·2	1·8	0·2	0·4	0·0	93·4	34·4
297-06	4·8	8·0	0·0	0·4	0·0	86·8	46·0
297-07	11·4	7·2	1·0	3·6	0·0	76·8	32·0
297-09	3·4	3·6	0·0	0·0	0·0	93·0	5·2
297-10	0·0	0·8	0·0	0·0	0·0	99·2	44·0
297-11	0·0	0·4	0·0	0·0	0·0	99·6	39·2
297-14	1·6	4·0	0·0	2·8	0·0	91·6	4·6
297-17	3·6	4·4	0·0	4·8	1·2	86·0	27·6
297-18	1·6	0·4	0·2	0·0	0·0	97·8	32·6
297-25	6·4	3·2	0·0	1·4	0·6	88·4	30·6
297-26	10·4	2·8	0·0	5·2	1·0	80·6	2·0
297-27	36·2	5·8	2·2	0·0	0·0	55·8	10·4
298-12	1·6	5·4	0·0	0·0	0·0	93·0	<0·1
298-16	0·6	0·2	<0·1	<0·1	0·0	99·2	<0·1
298-19	26·2	2·4	<0·1	<0·1	0·0	71·4	<0·1
298-20	5·2	5·0	0·0	0·0	0·0	89·8	<0·1
299-02	13·6	1·0	<0·1	0·0	0·0	85·4	2·6
299-04	0·0	0·0	0·0	0·0	0·0	100·0	27·2
299-05	0·8	6·8	0·0	0·0	0·0	92·4	44·0
299-12*	0·8	1·8	0·0	0·4	0·0	97·0	<0·1
299-14*	0·0	0·2	0·0	0·2	0·0	99·6	18·2
299-15*	0·0	0·0	0·0	0·2	<0·1	99·8	<0·1
299-20*	2·4	1·6	0·0	0·0	0·2	95·8	<0·1
299-21*	11·4	7·2	0·0	0·4	0·0	81·0	<0·1
299-23*	0·2	2·2	0·0	0·2	0·0	97·4	0·8
299-27*	0·6	1·4	0·0	0·4	0·0	97·6	14·4
299-28	0·0	0·4	0·0	0·8	0·0	98·8	25·2
299-29*	1·6	0·8	0·0	1·2	0·0	96·4	3·6
299-33	0·6	2·8	0·0	2·4	1·0	93·2	<0·1
299-37	2·8	2·0	0·0	0·0	0·0	95·2	8·6
KS1-10	2·4	1·2	0·0	0·6	0·8	95·0	3·8
KS1-13	23·8	7·8	1·2	0·0	0·0	67·2	0·4
KS1-19	5·6	3·4	<0·1	<0·1	0·0	91·0	0·6
KS3-1	0·2	0·6	0·0	0·0	0·2	99·0	1·6
KS3-3	5·6	8·4	0·4	0·0	0·0	85·6	<0·1
Mean	5·2	3·0	0·2	0·8	0·1	90·7	12·9
Alkalic and transitional lavas							
297-19	3·4	4·0	0·0	0·0	0·0	92·6	8·4
297-20	9·2	8·2	0·0	0·0	0·0	82·6	1·0
297-21	2·2	3·4	0·0	0·0	0·0	94·4	2·0
297-22	1·4	4·2	0·0	0·2	0·0	94·2	0·4
297-23	1·4	0·8	<0·1	0·0	0·0	97·8	<0·1
297-24	2·6	1·0	<0·1	0·0	0·0	96·4	<0·1
KS2	1·8	3·2	0·0	0·0	0·0	95·0	2·0
Mean	3·1	3·5	0·0	0·0	0·0	93·4	2·8

*Orthopyroxene in matrix.
plag, plagioclase; cpx, clinopyroxene; ph, phenocryst; mph, microphenocryst; xeno, xenocryst.

submarine environment. Others have a coarse-grained groundmass with sub-ophitic texture suggesting slow cooling, perhaps within a flow interior. The total olivine content (phenocrysts, >0·5 mm in diameter, xenocrysts with resorbed margins with strong sub-grain dislocations, plus microphenocrysts 0·1–0·5 mm in diameter) in SKS lavas shows dramatic variations (0·0–44·2 vol. % olivine), although most samples contain <10 vol. % olivine (mean value is 7·6 vol. %; Table 1). Several samples contain strongly elongate olivine (Fig. 3), which is common in submarine quenched Hawaiian lavas (e.g. Mauna Loa volcano; Davis *et al.*, 2003). Spinel commonly occurs as inclusions in SKS olivine and rarely as microphenocrysts (0·1–0·5 mm). Phenocrysts of plagioclase and pyroxene are absent in SKS lavas (Table 1). Plagioclase microphenocrysts are found in most lavas (54%), although they are usually rare (<1 vol. %). Clinopyroxene microphenocrysts are present in 22% of the samples, usually occurring with plagioclase microphenocrysts (Table 1). The greater abundance of microphenocrysts of plagioclase compared with clinopyroxene is an indication that plagioclase formed earlier in SKS lavas. This crystallization sequence is common in lavas from Mauna Loa but not those from Kīlauea, which have a distinct bulk composition from Mauna Loa lavas (e.g. Macdonald, 1949; Montierth *et al.*, 1995). Orthopyroxene crystals are common (2–4 vol. %) in the groundmass of most samples from dive 299; otherwise they are absent in SKS lavas (Table 1). Nepheline crystals were found only in the matrix of sample KS2.

METHODS

Olivine compositions were measured with a five-spectrometer JEOL 8500F Hyperprobe at the University of Hawai`i for 21 SKS volcanic rocks using moderately precise but rapid methods to allow for a broad survey. These analyses were made using 20 kV, a beam current of 40 nA, and a beam diameter of 10 μm. The peak and background counting times were 30 s each for all elements. The 2σ precision based on counting statistics is <1% for SiO_2, MgO and FeO, and 2–4% for CaO and NiO. Three spot analyses were averaged for core composition and one spot for rims. For the high-precision analyses, higher current (200 nA) and longer counting times (100 s for Ni, Ca, Mg and Si, and 60 s for Mn and Fe) on large crystals for Ni, Ca and Mn resulted in greater precision data (2σ errors are <0·03 wt % for SiO_2, MgO and FeO and <0·01 for CaO, MnO and NiO based on replicate analyses of the Smithsonian San Carlos Olivine standard) than our other olivine analyses (Supplementary Data Electronic Appendix 3). The standards for all analyses were USNM San Carlos olivine (forsterite 90%) for Si, Fe and Mg, titanite glass for Ca, and synthetic NiO for Ni. San Carlos olivine was also used as an internal control to check instrument drift and reproducibility. Oxygen was calculated by cation stoichiometry and used in the PAP-ZAF matrix correction for determining final analyses. Oxide concentrations were calculated using the procedures of Armstrong (1988). Typically, 25 olivines were analyzed per sample (where possible) resulting in data for 506 olivines (Supplementary Data Electronic Appendix 3 presents representative analyses for 10 olivines per sample).

Whole-rock XRF analyses were made on all of the unaltered or weakly altered (i.e. thin, <0·01 mm, iddingsite rims on olivine and no secondary minerals in vesicles) SKS basalt samples as well as some of the moderately altered (thicker iddingsite rims and/or clay or zeolite lining on vesicles) samples (53 samples from 19 areas). Samples were extensively washed prior to analysis using the protocol developed for the HSDP drill core (Rhodes, 1996). The crushed material was washed by percolating water through it until the water had the conductivity of the tap water (~100 microsiemens). This procedure took 2–7 days. Samples were then cleaned in an ultrasonic bath with deionized (D.I.) water for intervals of 2–5 min, depending on how quickly the water turned cloudy, until the conductivity of the water was less than two microsiemens. Samples were then dried overnight at 120°C and cooled. Splits of the samples were powdered using a tungsten-carbide coated mill, dried overnight at 120°C, cooled and weighed before drying in an oven at ~1000°C overnight to determine loss on ignition (LOI). The oxidized powders were analyzed by XRF for major and trace elements at the University of Massachusetts [see Rhodes (1996) and Rhodes & Vollinger (2004) for analytical procedures and precision].

Trace element analyses by ICP-MS were carried out at the Pacific Centre for Isotope and Geochemical Research (PICGR), University of British Columbia, following the methods described by Pretorius *et al.* (2006) and Carpentier *et al.* (2013).

High-precision Pb, Sr, Nd and Hf isotopic data were collected for 19 SKS samples. Samples were carefully acid-leached to minimize post-eruptive alteration affects (Weis *et al.*, 2005; Nobre Silva *et al.*, 2009, 2010). After a 48 h period of digestion in concentrated sub-boiled HF and HNO_3 and a 24 h period of digestion in 6 N sub-boiled HCl, samples were purified using Pb, Sr, Nd and Hf anionic exchange columns to separate these elements [see Weis *et al.* (2006, 2007) and Connelly *et al.* (2006) for detailed procedure]. The Pb, Nd and Hf isotopes were analyzed by multicollector (MC)-ICP-MS using a Nu Plasma NU 021 system. Sr isotopes were analyzed by thermal ionization mass spectrometry (TIMS) using a Finnigan Triton system, both at the PCIGR. Complete procedural duplicates were analyzed for sample J2-297-23 yielding an external reproducibility for the Pb, Sr, Nd and Hf of 69–131, 5–22, 1 and 16 ppm, respectively. During this study, the NBS 987 standard gave $^{87}Sr/^{86}Sr = 0{\cdot}710253 \pm 13$ ($n = 7$); La Jolla Nd: $^{143}Nd/^{144}Nd = 0{\cdot}511853 \pm 11$ ($n = 11$); JMC 475: $^{176}Hf/^{177}Hf = 0{\cdot}282154 \pm 29$ ($n = 13$), and SRM 981: $^{206}Pb/^{204}Pb = 16{\cdot}9425 \pm 17$, $^{207}Pb/^{204}Pb = 15{\cdot}5002 \pm 21$, $^{208}Pb/^{204}Pb = 36{\cdot}7222 \pm 60$ ($n = 20$). The BHVO-2 USGS standard was analyzed together with the samples and the results are within error of the published values (Weis *et al.*, 2006, 2007). Five samples were replicated (solution was re-analyzed) and one was completely duplicated.

OLIVINE COMPOSITIONS

Olivine core compositions in SKS lavas range widely (74–90% forsterite, Fo; Fig. 5; Supplementary Data Electronic Appendix 3). Phenocrysts and xenocrysts (i.e.

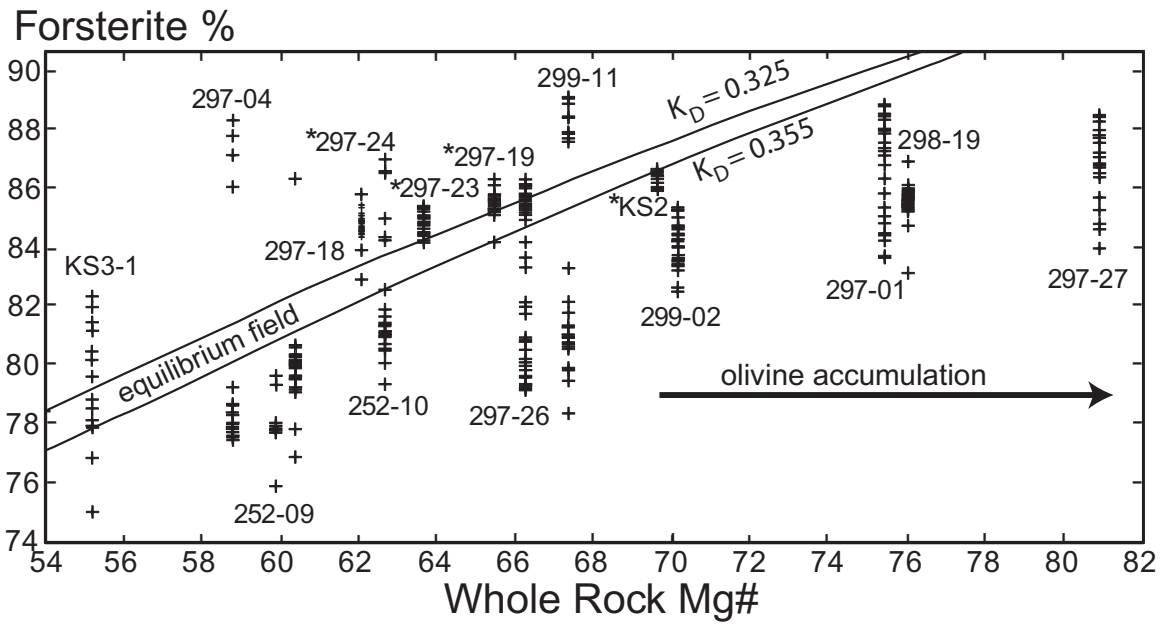

Fig. 5. South Kaua`i Swell whole-rock Mg# [100Mg/(Fe^{2+} + Mg)] assuming 10% of the total iron is oxidized versus olivine composition (forsterite per cent) for selected samples. Olivine analyses are stacked vertically for each sample with a plus mark for each crystal (average of three spot analyses). (See Supplementary Data Electronic Appendix 3 for representative olivine data.) The paired diagonal lines are the equilibrium field using a value of 0·340 ± 0·015 reflecting work of Putirka *et al.* (2007) and Matzen *et al.* (2011). Some olivines plot below the equilibrium field, reflecting accumulation of olivine causing an increase in the rock Mg#. Olivines that plot above the field may be xenocrysts, crystals from a more Mg-rich magma that were mixed with lower Mg# magma or early formed crystals that were not completely separated.

kink-banded or resorbed margins) have the same range in Fo (78–90%), whereas microphenocryst compositions extend to lower Fo values (74%). Olivine rim compositions vary from 67 to 89% Fo. Nearly all of the olivines have normal zoning or are unzoned. Only a few samples have reversely zoned crystals and the extent of their zoning is small (usually <1% Fo). The SKS olivine core compositions are identical to those reported for other Hawaiian volcanoes (e.g. Kīlauea: 78–90% Fo, Clague *et al.*, 1995; Ko`olau: 78–90% Fo; Garcia, 2002). There is a bimodal distribution in Fo content of SKS olivine cores with peaks at 81 and 86%, which is similar to but slightly lower than those reported for Kīlauea submarine lavas (82–83 and 88–89%; Clague *et al.*, 1995). Some SKS samples display bimodal olivine compositions (with a gap of 4–5% Fo) and others have large ranges in Fo (>4%; Fig. 5). Bimodal populations, clustering above and below the equilibrium field, were found in samples 299-11 and 297-04 (Fig. 5). Both groups of olivines have normal or no zoning. Thus, if magma mixing was responsible for the bimodal olivine compositions, it occurred during or just before eruption. The samples with large ranges in Fo content probably picked up olivine during magma ascent, as seen in lavas from other Hawaiian volcanoes (e.g. Mauna Kea; Garcia, 1996).

The Fo content of olivines in most SKS samples is out of equilibrium with the whole-rock composition (Fig. 5). Only five of 21 samples (including all four of the analyzed alkalic rocks) have olivines that plot near or within the equilibrium field (Fig. 5). Olivines from five other samples plot entirely below the equilibrium field. Four of these samples have whole-rock Mg#s [100Mg/(Fe^{2+} + Mg)] of 70–81 (assuming 90% of whole-rock total iron is Fe^{2+}), the highest Mg#s among the studied SKS samples. Comparably high Mg#s have also been found in submarine lavas from Mauna Loa, Ko`olau and Mauna Kea, and were interpreted to result from accumulation of olivine (e.g. Garcia, 1996, 2002). The Fo contents of some SKS olivines plot above the equilibrium field (Fig. 5). These olivines may be relics of earlier crystallization and were not removed by fractionation (e.g. Maaløe *et al.*, 1988).

The CaO content of SKS olivines increases with decreasing Fo (Supplementary Data Electronic Appendix 3), whereas NiO content decreases (Fig. 6). Both are common features in volcanic rocks (e.g. Nakamura, 1995; Libourel, 1999). The SKS tholeiitic lavas have lower CaO and higher NiO at a given Fo content than the alkalic lavas (Fig. 6; Supplementary Data Electronic Appendix 3). The amounts of NiO (Fig. 6) and CaO in olivines from SKS tholeiites are relatively high and low, respectively, at a given Fo value for Hawaiian lavas, which is similar to olivines in lavas from Loa-trend volcanoes (e.g. Ko`olau and Mauna Loa; Garcia, 2002; Sobolev *et al.*, 2007).

WHOLE-ROCK COMPOSITIONS

Major and trace elements

The SKS rocks are all basalts, ranging in composition from basanite and picro-tholeiitic basalt to tholeiitic

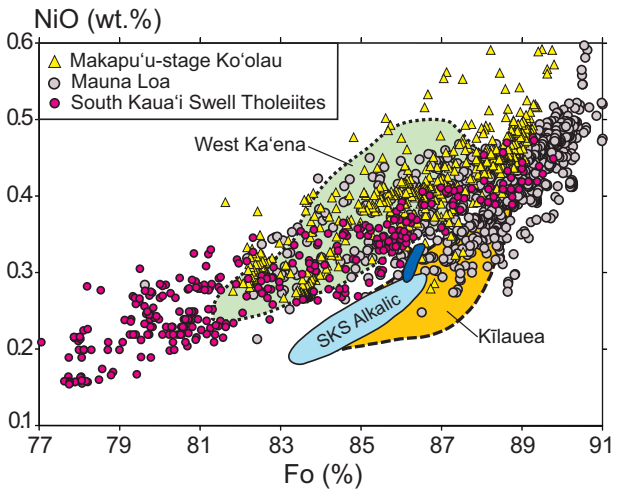

Fig. 6. Plot of forsterite (Fo%) and Ni content in SKS olivines (red circles, tholeiitic lavas; dark blue field, older alkalic lava KS2; light blue field, young alkalic lavas) compared with olivines from other Hawaiian volcanoes [gray circles, Mauna Loa; yellow triangles, Makapu'u stage of Ko`olau; gold field, Kīlauea; all data from Sobolev *et al.* (2007); light green field, West Ka`ena (Greene *et al.*, 2010)]. All of the other volcanoes are from the Loa-trend except Kīlauea. (See Supplementary Data Electronic Appendix 3 for olivine data.)

basalt (Fig. 7). The alkalic rocks ($n = 6$) were collected on the northern flank of the SKS (dive 297 and dredge KS2; Fig. 2), whereas the tholeiitic lavas are widespread. One transitional lava (sample 297-24) was recovered during dive 297 from the same area that yielded alkalic lavas. The young ages for the SKS alkalic and transitional lavas compared with the SKS tholeiitic lavas (0·08, 0·2 and 1·9 vs 3·9–5·4 Ma; Supplementary Data Electronic Appendix 2) indicate that the alkalic and transitional lavas were erupted during the rejuvenated stage. However, the young dive 297 samples are geochemically distinct compared with most other Hawaiian rejuvenated lavas (e.g. lower TiO_2, Ba and La/Yb, and higher Al_2O_3 at a given MgO value than Kōloa rejuvenated lavas from Kaua`i and the 1·9 Ma basanite KS2 (Figs 8 and 9), except those from Ni`ihau (see Cousens & Clague, in press).

The SKS tholeiites range widely in composition (e.g. 6–25 wt % MgO), although most have MgO concentrations <13 wt %, unlike many Kaua`i shield lavas (Fig. 8). The higher MgO contents of the Kaua`i shield lavas (up to 30 wt %) reflect substantial olivine addition based on their moderate olivine forsterite contents (e.g. 81–89%; e.g. Maaløe *et al.*, 1989). The SKS tholeiites with MgO > 13 wt % also have olivine Fo compositions too low to be in equilibrium with the host rock (Fig. 2). This indicates that these rocks accumulated olivine. The wide variations in TiO_2 and Zr/Nb at constant MgO in tholeiitic SKS lavas (Table 2, Figs 8 and 9) cannot be attributed to olivine addition or sample alteration. Instead, these variations reflect distinct parental magmas. Compositions of SKS tholeiites generally overlap with those for Kaua`i shield lavas, although some SKS samples have lower TiO_2 and Al_2O_3 at a given MgO

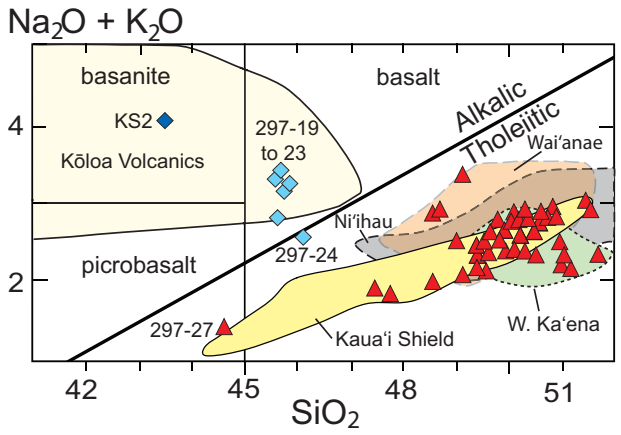

Fig. 7. Whole-rock total alkalis ($Na_2O + K_2O$) vs SiO_2 diagram for SKS lavas showing the Macdonald & Katsura (1964) alkali vs tholeiitic dividing line. Red triangles, SKS tholeiites; light blue diamonds, weakly alkalic and transitional SKS lavas; dark blue diamond, KS2 basanite. Most of the SKS lavas are tholeiitic in composition and are similar to Kaua`i shield lavas (yellow field). Most of the SKS alkalic lavas plot within the Kōloa Volcanics field (pale yellow field). Data for fields: Kaua`i shield and Kōloa Volcanics from Garcia *et al.* (2010) and Mukhopadhyay *et al.* (2003); W. Ka`ena (light green) from Greene *et al.* (2010); Ni`ihau (gray) from Cousens & Clague (in preparation); Wai`anae (brown) from Coombs *et al.* (2004). SKS data are from Table 2. The 2σ error bars are within the size of the symbol.

content (Fig. 8), suggesting variable degrees of melting and somewhat distinct sources.

All of the SKS samples (except the basanite KS2) are moderately enriched in incompatible trace elements (e.g. Sr, V, Zr; Tables 2 and 3), similar to the Kaua`i shield lavas (Fig. 9). However, the SKS tholeiitic samples have higher average Sr/Y and Zr/Nb than the Kaua`i shield lavas (Fig. 9). Multiple tholeiitic samples from some SKS seamounts show a small range in trace element ratios, whereas other seamounts have a larger range (e.g. Zr/Nb, seamount 7B has 11·5–12·2 for six samples vs seamount 9C, 10·1–13·3 for three samples; Table 2). The young, weakly alkalic samples have lower La/Yb and Ba concentrations but similar Zr/Nb and Sr/Y compared with Kōloa rejuvenated lavas from Kaua`i (Fig. 9). The basanite sample KS2 shows strong incompatible element enrichment, similar to Kōloa lavas (Fig. 9).

The rare earth element (REE) patterns for the SKS tholeiitic lavas are relatively smooth (even on a linear scale plot; Fig. 10). The patterns fan out from a tight cluster for the heavy REE (HREE) and show moderate light REE (LREE) enrichment with a two-fold variation in La (Fig. 10). The small variation in HREE is typical of lavas from Hawaiian shield volcanoes and has been interpreted as indicating the presence of garnet in the source (e.g. Kohala, Lanphere & Frey, 1987; Lō`ihi, Garcia *et al.*, 1995). The young alkalic SKS lavas overlap but crosscut and have steeper LREE to moderate sloping REE patterns (La/Sm) than some of the SKS tholeiites, indicating distinct sources for the young alkalic

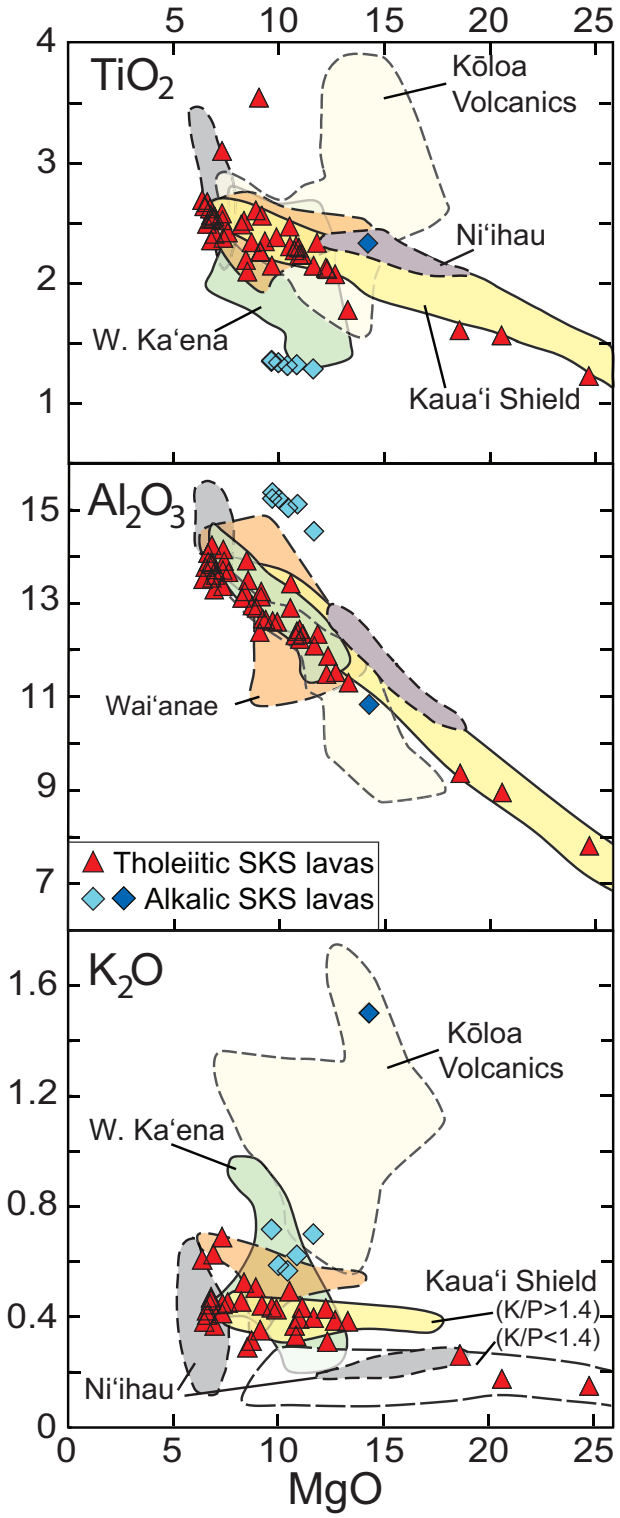

Fig. 8. Variation diagrams for TiO_2, Al_2O_3 and K_2O vs MgO (wt %) for the SKS lavas. The SKS tholeiites have somewhat lower TiO_2 and Al_2O_3 than Kaua`i shield lavas, whereas the young SKS alkalic lavas (light blue diamonds) are distinct from the Kōloa Volcanics in TiO_2 and Al_2O_3. Symbols, fields and data sources as in Fig. 7. SKS data are from Table 2. The 2σ error bars are within the size of the symbol.

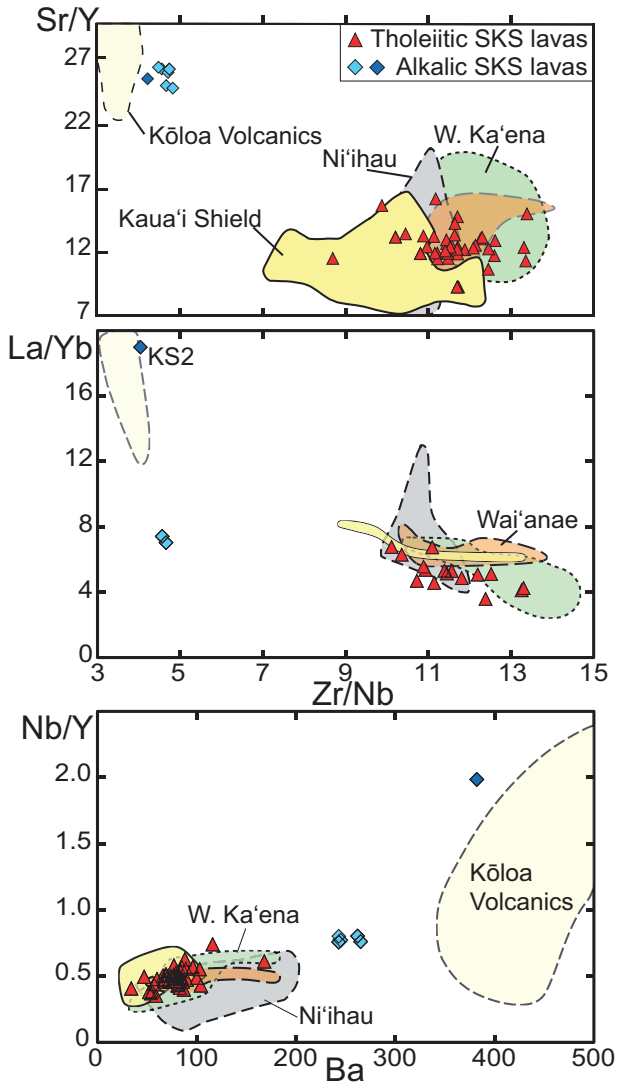

Fig. 9. Incompatible trace element variation diagrams for SKS lavas. The SKS tholeiites have somewhat lower La/Yb and Nb/Y at a given Ba and higher Zr/Nb than Kaua`i shield lavas but overlap the field for Ni`ihau, W. Ka`ena and Wai`anae. The young alkalic lavas (light blue diamonds) are distinct from the Kōloa Volcanics with lower Ba and La/Yb, but slightly higher Zr/Nb. Symbols, fields and data sources as in Fig. 7. SKS data are from Table 3. The 2σ error bars are within the size of the symbol.

lavas (Fig. 10). The REE pattern for the strongly alkalic sample (KS2) crosscuts all other patterns and shows marked LREE enrichment (Fig. 10), which is typical of Hawaiian rejuvenated lavas (e.g. Clague & Frey, 1982; Garcia *et al.*, 2010).

Isotopes

New high-precision Pb, Sr, Nd and Hf isotopic data were collected for 19 SKS samples (16 tholeiites and three alkalic lavas; Table 4). Two distinct groups are evident in the Sr, Nd and Hf isotopic data reflecting the tholeiitic and alkalic rock groups. The alkalic lavas have relatively low $^{87}Sr/^{86}Sr$ and high ε_{Hf} and ε_{Nd} ratios compared with the SKS tholeiites and Kaua`i shield lavas and are similar to the rejuvenated lavas from Kaua`i (Kōloa) and Ni`ihau (Figs 11 and 12). The weakly alkalic lavas have somewhat less radiogenic Pb isotopic compositions than the SKS tholeiitic lavas, whereas the basanite sample KS2 has a much higher $^{206}Pb/^{204}Pb$ ratio and overlaps with the tholeiites (Fig. 11; Table 4). The SKS tholeiites are very similar in Pb, Sr and Nd isotope ratios to the tholeiitic lavas from the nearby islands of Kaua`i, Ni`ihau and even those from Wai`anae volcano, ~140 km to the SE (Figs 11 and 12), although the Wai`anae lavas have generally less radiogenic Pb isotope ratios as well as higher Sr isotopic compositions. The overlap with Kaua`i shield lavas is excellent in all isotope systems, with a slight shift towards higher $^{208}Pb/^{204}Pb$ for a given $^{206}Pb/^{204}Pb$ compared with the data of Mukhopadhyay *et al.* (2003). The SKS tholeiites show only minor overlap in Pb, Sr, Nd and Hf isotope composition with lavas from West Ka`ena, which are distinctive with generally very unradiogenic Pb isotope ratios and high ε_{Nd} (Fig. 11).

LOCAL VS LANDSLIDE ORIGIN FOR SKS VOLCANICS

The gap in the ancient shoreline along the south coast of the Island of Kaua`i (white dotted line in Fig. 2) indicates that landslide debris were shed from the island onto the SKS (Ito *et al.*, 2013). Thus, some of the rocks we collected from the SKS may actually be of landslide origin from Kaua`i. To help distinguish these transported Kaua`i lavas from those that were erupted underwater at depths of >2 km from the SKS volcano, we examined the texture, vesicularity and geochemistry of the SKS lavas.

Texture and vesicularity implications

All of the alkalic SKS lavas have a glassy groundmass (Fig. 3), which indicates rapid quenching. All but one of these lavas are poorly vesicular (≤2·0 vol. %; Fig. 4; Table 1). The alkalic rock with higher vesicularity (8 vol. %; Fig. 4) was collected from the same cone as the other dive 297 alkalic lavas, and is petrographically and geochemically identical to those lavas (Tables 1 and 2; Supplementary Data Electronic Appendix 2). Observations from the videotapes taken during the JASON dive indicate that these samples were collected in place and have not been transported. The older (1·9 Ma) basanite was dredged from a 200 m tall, flat-topped cone and probably was recovered in place. The landslide scar on south Kaua`i is partially covered with up to 200 m of rejuvenated lavas (Garcia *et al.*, 2010). Thus, the south Kaua`i landslide probably occurred during or near the end of Kaua`i's shield development (3·6–4·0 Ma; Garcia *et al.*, 2010). Landslides also formed on other Hawaiian shield volcanoes at the end of the shield stage (e.g. East Moloka`i; Moore *et al.*, 1994). No major landslide is known to have occurred on any

Table 2: XRF major element oxide (wt %) and trace element (ppm) compositions for selected SKS lavas and volcanic breccias

	Tholeiites														
Sample:	252-02	252-04	252-05	252-07	252-09	252-10	297-01	297-02	297-04	297-05	297-06	297-07	297-09	297-10	297-11
SiO_2	49·6	50·85	49·46	49·27	50·32	49·59	48·58	51·68	50·60	49·43	49·94	49·04	49·97	50·85	50·49
TiO_2	2·312	2·536	2·276	2·338	2·343	2·385	1·832	2·583	2·491	2·119	2·237	2·077	2·242	2·496	2·624
Al_2O_3	12·40	13·54	12·31	12·34	12·95	12·6	9·74	13·71	13·11	11·87	12·23	11·52	12·34	14·07	13·87
Fe_2O_3	12·73	12·24	12·87	12·36	12·82	12·95	12·85	11·28	12·67	12·39	12·59	13·11	12·37	12·20	12·64
MnO	0·19	0·18	0·20	0·20	0·30	0·18	0·17	0·18	0·18	0·18	0·19	0·19	0·19	0·18	0·19
MgO	10·81	6·78	10·74	11·8	8·70	9·88	18·25	7·30	8·21	12·29	10·95	12·66	11·10	6·59	6·73
CaO	9·64	10·40	9·74	9·31	10·05	9·60	5·56	10·77	9·83	9·14	9·38	8·74	9·34	10·54	10·64
Na_2O	1·72	2·44	2·05	1·93	1·98	2·21	1·88	1·99	2·27	2·01	2·24	2·11	1·94	2·51	2·17
K_2O	0·333	0·472	0·370	0·252	0·315	0·429	0·974	0·415	0·457	0·311	0·395	0·388	0·435	0·425	0·447
P_2O_5	0·235	0·249	0·231	0·250	0·224	0·252	0·176	0·253	0·258	0·216	0·225	0·208	0·231	0·251	0·260
Total	99·97	99·67	100·25	100·05	100·00	100·08	100·02	100·17	100·08	99·96	100·38	100·05	100·16	100·11	100·06
LOI	0·29	0·15	0·15	0·27	0·23	0·09	5·1	0·32	0·15	0·08	−0·07	−0·12	−0·16	−0·03	0·31
Rb		6·2	5·2	3·2	4·6	6·5	10·4	5·2	6·1	4·4	5·9	5·7	6·0	6·3	6·7
Sr		319	305	305	300	331	209	314	320	286	286	266	290	325	328
Ba		77	80	90	86	96	74	60	68	67	80	76	84	78	89
V		277	240	232	254	246	174	270	250	228	241	227	240	260	276
Cr		275	573	627	467	475	930	375	396	678	688	743	587	239	194
Ni		76	274	431	182	192	745	136	171	398	308	393	354	78	83
Zn		118	127	124	125	124	124	113	126	118	119	124	117	117	126
Ga		20	19	19	20	19	14	20	20	18	18	17	18	20	20
Y		25·7	23·2	24·8	25·0	24·6	17·5	25·8	24·5	21·7	23·0	21·8	23·1	25·7	26·4
Zr		150	125	145	129	145	98	151	150	126	135	124	134	148	160
Nb		13·1	11·3	11·7	11·4	14·0	8·8	12·3	12·3	10·3	11·6	10·5	11·1	12·9	14·7
La		8	8	10	9	5	4	6	8	7	9	8	8	8	9
Ce		27	27	27	38	29	18	25	29	21	24	23	23	26	29

	Tholeiites															
Sample:	297-14	297-17	297-18	297-25	297-26	297-27	298-07	298-12	298-16	298-19	298-20	299-02	299-04	299-05	299-08	299-12
SiO_2	50·24	48·59	51·01	49·41	49·81	44·64	51·47	50·18	50·43	47·76	49·98	49·12	50·93	49·59	51·11	50·08
TiO_2	2·266	2·309	2·099	2·299	2·474	1·229	2·694	2·564	2·425	1·611	2·608	1·779	2·359	2·195	2·413	2·149
Al_2O_3	13·14	13·42	13·49	12·44	12·90	7·81	13·51	12·67	13·66	9·36	12·90	11·30	14·24	13·91	13·6	12·62
Fe_2O_3	12·45	12·87	12·26	12·14	11·76	12·79	12·12	12·71	11·79	13·01	12·42	12·40	12·26	11·62	12·49	12·55
MnO	0·19	0·20	0·18	0·18	0·16	0·17	0·20	0·18	0·18	0·18	0·18	0·21	0·18	0·17	0·19	0·18
MgO	9·11	10·52	8·50	10·94	10·50	24·69	6·36	9·19	7·57	18·56	8·90	13·26	6·78	8·43	6·95	9·66
CaO	10·15	10·00	10·05	9·73	9·37	7·10	10·43	9·62	10·70	7·54	10·22	9·41	10·72	11·26	10·79	10·19
Na_2O	2·22	1·74	1·91	2·17	2·28	1·26	2·40	2·31	2·31	1·58	2·22	1·60	2·21	1·87	1·88	2·04
K_2O	0·353	0·212	0·291	0·277	0·494	0·159	0·609	0·443	0·453	0·264	0·507	0·385	0·293	0·210	0·30	0·436
P_2O_5	0·214	0·211	0·192	0·231	0·310	0·191	0·261	0·268	0·241	0·155	0·269	0·195	0·232	0·225	0·233	0·199
Total	100·33	100·07	99·98	99·82	100·06	100·04	100·05	100·13	99·76	100·02	100·20	99·66	100·21	99·48	99·96	100·10
LOI	0·05	0·56	−0·07	−0·04	0·12	0·77	0·76	0·39	0·44	1·29	0·70	2·81	0·61	1·65	0·92	1·04
Rb	4·7	2·7	3·5	3·7	7·0	2·6	11·2	7·3	5·4	4·0	6·0	3·2	4·0	3·1	3·7	7·6
Sr	280	299	286	306	378	200	326	345	326	203	347	205	292	275	300	275
Ba	67	80	55	67	88	34	83	77	71	83	103	54	87	59	57	82
V	245	253	220	240	215	154	294	236	249	172	246	251	261	259	280	226
Cr	527	558	423	632	576	1918	129	534	357	1226	540	1250	174	487	270	637
Ni	225	279	153	329	364	1263	133	193	153	922	242	421	80	175	89	239
Zn	118	127	110	118	120	112	121	128	108	119	118	130	118	168	116	116
Ga	19	20	20	19	19	11	21	21	20	14	21	16	21	19	19	19
Y	24·3	25·2	23·1	24·1	23·3	13·3	28·4	23·3	24·4	17·3	24·3	22·7	27·4	29·7	25·5	22·3
Zr	130	135	118	125	162	72	156	157	141	89	155	108	135	121	134	119
Nb	11·4	11·6	8·9	11·0	14·6	5·4	14·0	13·5	12·2	7·1	13·4	8·4	10·9	10·4	11·2	9·9
La	8	11	8	8	9	5	9	9	8	5	11	7	8	9	9	9
Ce	26	26	23	26	31	15	28	30	27	17	28	24	24	25	24	27

(continued)

Table 2: Continued

	Tholeiites														
Sample:	299-14	299-15	299-20	299-21	299-23	299-27	299-28	299-29	299-33	299-37	KS1-10	KS1-13	KS1-19	KS3-1	KS3-3
SiO_2	50·56	51·04	51·62	49·84	49·14	50·78	50·07	50·32	50·64	50·02	48·72	47·49	50·11	50·88	49·48
TiO_2	2·379	2·643	2·544	2·131	3·102	2·558	2·676	2·526	2·521	2·265	3·547	1·568	2·351	2·570	2·148
Al_2O_3	13·90	13·77	13·29	11·48	13·36	13·72	13·89	14·15	13·25	13·25	12·38	8·95	12·65	13·83	12·09
Fe_2O_3	12·11	12·27	12·36	12·37	13·32	12·38	12·48	12·06	12·14	12·23	13·24	12·58	12·76	12·13	12·60
MnO	0·19	0·18	0·19	0·17	0·19	0·20	0·19	0·18	0·18	0·18	0·21	0·17	0·20	0·19	0·18
MgO	7·36	6·46	6·89	12·22	7·30	6·95	6·60	7·32	8·34	9·12	9·05	20·55	9·33	6·78	11·64
CaO	11·06	10·79	9·98	8·90	10·09	10·55	10·64	10·50	10·02	10·42	9·59	6·95	10·27	10·66	9·25
Na_2O	2·06	1·92	2·25	2·07	2·62	2·42	2·40	2·44	2·31	2·22	2·47	1·71	2·13	2·31	2·08
K_2O	0·256	0·384	0·628	0·431	0·690	0·370	0·409	0·448	0·525	0·213	0·419	0·172	0·281	0·462	0·398
P_2O_5	0·228	0·26	0·259	0·212	0·335	0·251	0·269	0·250	0·259	0·206	0·402	0·149	0·22	0·255	0·219
Total	100·10	99·72	100·01	99·82	100·15	100·18	99·63	100·19	100·18	100·12	100·03	100·29	100·30	100·07	100·08
LOI	0·51	−0·16	0·58	1·24	0·15	−0·01	−0·01	−0·17	0·51	1·45	1·77	0·92	0·86	−0·53	−0·01
Rb	3·3	4·9	9·2	7·9	10·2	5·5	5·7	6·2	9·4	1·5	3·4	2·2	3·8	7·7	5·5
Sr	316	322	292	283	383	335	346	347	328	285	391	200	284	334	273
Ba	81	72	81	104	168	85	79	84	100	52	116	47	69	85	66
V	255	283	261	208	292	250	271	248	253	228	323	185	250	265	224
Cr	310	164	343	839	444	247	232	285	460	575	343	978	596	239	792
Ni	100	74	98	485	143	89	85	116	201	220	241	1018	256	84	335
Zn	111	113	120	118	125	111	126	115	117	146	146	113	124	111	114
Ga	20	21	20	19	24	21	21	20	21	20	23	14	19	20	17
Y	25·8	26·5	25·8	21·9	29·0	25·8	27·0	24·2	25·3	24·3	34·6	16·8	23·6	25·2	22·9
Zr	129	154	149	118	179	142	150	141	154	118	215	89	134	155	131
Nb	11·1	12·2	11·2	9·4	17·7	12·5	14·2	12·9	12·3	9·2	25·6	8·3	12·1	14·3	11·5
La	10	10	7	6	14	10	10	11	10	8	21	6	6	13	7
Ce	29	31	23	25	42	31	28	31	28	23	58	16	26	33	21

	Alkalic basalts							International standard	
Sample:	297-19	297-20	297-21	297-22	297-23	297-24	KS2	BHVO-2	1 SD
SiO_2	45·82	45·66	45·91	45·63	45·71	46·14	43·53	49·84	0·05
TiO_2	1·323	1·288	1·351	1·340	1·316	1·359	2·342	2·728	0·005
Al_2O_3	15·12	14·54	15·24	15·23	15·04	15·37	10·84	13·53	0·05
Fe_2O_3	12·55	13·03	12·92	12·98	13·05	12·96	13·71	12·22	0·024
MnO	0·19	0·20	0·20	0·20	0·21	0·19	0·19	0·183	0·003
MgO	10·84	11·62	9·64	9·97	10·40	9·65	14·24	7·123	0·07
CaO	11·08	10·72	11·20	11·12	10·94	11·45	10·69	11·35	0·03
Na_2O	2·54	2·13	2·55	2·73	2·80	2·18	2·51	2·04	0·263
K_2O	0·624	0·701	0·718	0·588	0·568	0·420	1·502	0·514	0·003
P_2O_5	0·264	0·259	0·296	0·291	0·292	0·297	0·423	0·271	0·002
Total	100·35	100·15	100·025	100·08	100·33	100·02	99·98	99·83	0·259
LOI	0·50	0·61	0·60	0·33	0·19	1·20	1·62	—	—
Rb	9·4	10·8	11·7	8·5	8·8	7·0	20·0	7·6	0·6
Sr	448	432	482	477	474	487	545	394	47
Ba	243	243	262	244	245	265	382	131	4
V	235	227	238	235	237	239	218	288	4·2
Cr	472	499	420	422	437	358	628	296	3·8
Ni	246	269	207	206	228	179	370	113	0·7
Zn	97	95	97	96	96	94	118	110	0·7
Ga	16	16	16	16	16	17	16	20·8	0·43
Y	17·8	17·3	18·2	18·2	17·9	18·4	21·2	25·0	0·23
Zr	62	61	64	64	63	64	170	177·8	2·3
Nb	13·8	13·1	14·6	14·1	13·8	14·0	42·1	18·28	0·2
La	10	10	13	12	10	13	21	14	2
Ce	27	25	30	29	27	31	53	38	2

All iron analyzed as Fe_2O_3. LOI, loss-on-ignition; BHVO-2 standard averages are based on 21 analyses for major elements and 40 analyses for trace elements.

Table 3: ICP-MS analyses of SKS lavas (values in ppm)

	Tholeiites											
Sample:	252-04	252-10	297-04	297-07	297-11	297-18	297-26	298-07	298-20	299-04	299-20	299-23
Sc	31·6	29·0	27·8	25·9	31·0	29·0	23·7	31·8	27·6	31·1	29·4	29·7
Ni	75	231	151	451	83	183	313	117	215	74	92	172
Ga	18·8	17·1	20·0	16·8	19·9	19·3	18·1	19·6	18·6	18·3	17·5	20·9
Y	26·2	24·5	23·9	21·2	25·8	22·3	22·8	27·6	23·6	26·2	24·0	26·6
Zr	142	129	144	112	145	109	172	160	167	140	151	164
Ba	77	83	79	73	91	61	104	87	94	92	80	134
Nb	11·5	11·8	10·9	9·6	13·0	8·2	14·2	13·7	14·0	11·0	11·1	16·3
Cs	0·21	0·20	0·06	—	—	—	0·08	0·43	0·10	0·07	0·21	0·08
Ta	1·32	1·14	0·80	0·78	1·00	0·64	1·15	1·09	1·10	0·93	0·95	1·35
Th	0·74	0·86	0·74	0·62	0·85	0·53	0·93	0·82	0·83	0·64	0·66	1·08
U	0·22	0·25	0·24	0·20	0·25	0·16	0·32	2·11	0·29	0·20	0·26	0·38
La	11·0	12·6	10·2	8·7	12·0	7·7	12·6	11·1	10·8	8·9	8·9	14·2
Ce	30·2	30·2	26·3	23·0	30·4	21·0	32·7	28·8	28·6	23·7	24·6	34·5
Pr	3·91	3·96	3·89	3·29	4·26	3·05	4·67	4·29	4·17	3·56	3·55	4·76
Nd	19·1	19·1	19·3	16·0	20·6	15·1	22·7	21·3	20·8	17·8	18·1	21·8
Sm	5·46	5·33	5·33	4·45	5·49	4·36	5·92	5·79	5·59	5·01	5·02	5·73
Eu	1·87	1·82	1·87	1·49	1·86	1·54	1·99	2·00	1·86	1·74	1·65	1·86
Gd	5·48	5·41	5·73	4·79	5·88	5·01	6·20	6·67	6·21	5·88	5·36	6·14
Tb	0·86	0·81	0·90	0·77	0·90	0·79	0·94	1·02	0·93	0·94	0·85	0·93
Dy	5·73	5·19	5·35	4·40	5·34	4·67	5·50	6·12	5·53	5·71	5·12	5·42
Ho	0·99	0·93	0·94	0·85	1·00	0·86	0·95	1·14	0·99	1·10	0·91	1·00
Er	2·56	2·36	2·57	2·22	2·81	2·21	2·47	3·17	2·68	3·04	2·56	2·68
Tm	0·28	0·25	0·32	0·29	0·34	0·30	0·31	0·39	0·33	0·38	0·34	0·34
Yb	2·14	2·01	2·00	1·80	2·16	1·88	1·87	2·44	2·04	2·48	2·09	2·10
Lu	0·31	0·27	0·27	0·26	0·30	0·27	0·25	0·33	0·28	0·34	0·28	0·29

	Tholeiites				Alkalic basalts				Standard values	
Sample:	299-29	299-33	KS1-13	KS3-3	297-20	297-23	297-23 (dup)	KS-2	Kil-93	Kil-93 (rep)
Sc	28·6	27·8	22·4	29·1	27·6	28·0	28·6	26·1	31·4	31·7
Ni	134	213	987	305	303	205	205	346	150	152
Ga	20·1	19·6	12·1	16·6	15·2	15·4	15·6	16·9	18·1	18·4
Y	23·5	24·2	16·6	23·8	16·9	17·8	18·1	21·6	18·1	18·4
Zr	139	145	80	120	57	69	69	158	139	140
Ba	83	97	40	68	238	265	269	425	95	98
Nb	12·3	11·1	7·2	9·9	11·9	14·5	14·5	34·3	13·6	12·8
Cs	0·07	0·43	0·25	0·20	—	0·26	0·24	0·44	0·04	0·07
Ta	0·93	0·84	0·98	0·87	0·74	1·17	1·02	2·57	0·95	0·97
Th	0·79	0·75	0·44	0·68	0·94	1·08	1·10	3·25	0·86	0·81
U	0·22	0·29	0·15	0·21	0·25	0·30	0·30	0·90	0·26	0·28
La	10·6	10·4	6·7	10·4	11·4	13·0	13·2	30·7	11·4	10·9
Ce	27·7	26·9	19·2	26·4	26·3	30·0	30·7	65·1	29·6	28·4
Pr	3·95	3·97	2·46	3·41	3·37	3·90	4·06	7·09	4·00	3·89
Nd	18·9	19·3	11·7	17·4	15·2	17·5	18·1	31·5	19·2	19·1
Sm	5·13	5·37	3·36	4·82	3·52	3·94	4·03	6·85	5·14	5·25
Eu	1·80	1·85	1·11	1·67	1·16	1·36	1·36	2·21	1·72	1·79
Gd	5·48	5·72	3·65	5·11	3·60	3·94	4·38	6·38	5·88	5·46
Tb	0·86	0·89	0·51	0·74	0·57	0·60	0·66	0·89	0·83	0·80
Dy	5·10	5·43	3·46	4·93	3·37	3·79	3·88	4·81	4·95	5·01
Ho	0·95	0·98	0·64	0·86	0·65	0·72	0·78	0·86	0·92	0·93
Er	2·41	2·59	1·66	2·29	1·86	1·99	2·20	2·03	2·41	2·36
Tm	0·32	0·33	0·20	0·28	0·25	0·27	0·28	0·25	0·32	0·31
Yb	1·98	2·05	1·43	1·95	1·62	1·75	1·78	1·62	2·09	2·07
Lu	0·28	0·29	0·21	0·27	0·23	0·26	0·26	0·20	0·27	0·27

Duplicate (dup) refers to independent sample processing; replicate (rep) refers to repeated measurement of the same solution on the MC-ICP-MS. Kil-93 is a Kīlauea tholeiite, similar in composition to BHVO-1, and has been described by Eggins *et al.* (1997).

Hawaiian volcano during or after rejuvenated volcanism (Sherrod *et al.*, 2007*b*).

Most SKS tholeiitic lavas have a fine-grained or glassy groundmass (Fig. 3) indicating they were rapidly quenched, presumably in a submarine setting. All of these samples were encased in thick Mn coatings (typically >1 cm), which made them difficult to collect. Vesicularity in the SKS lavas displays remarkable (<1 to 46 vol. %) and bimodal variations (Fig. 4). Hawaiian submarine tholeiitic lavas generally decrease in vesicularity with eruption depth (e.g. Moore, 1965). Notable exceptions include the vesicular submarine lavas sampled near submarine vents on Lō'ihi (e.g. 10–30 vol. % for tholeiitic lavas; Garcia *et al.*, 1995) and on the West

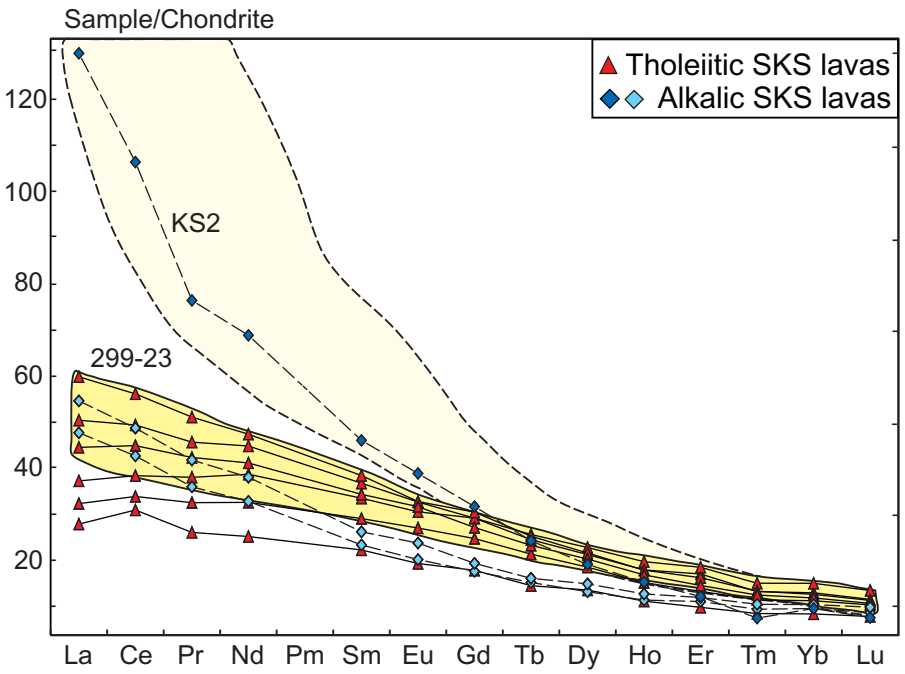

Fig. 10. Rare earth element (REE) diagram (ICP-MS data) for SKS volcanic rocks. REE values normalized to chondrite values from McDonough & Sun (1995). SKS tholeiitic and Kaua`i shield (darker yellow field) lavas are remarkably similar in their REE patterns. The basanite sample (KS2) plots within the rejuvenated Kōloa lava field (light yellow field). The tholeiitic and weakly alkalic lavas show a moderate LREE-enriched trend whereas the basanite is strongly enriched in LREE. The fanning LREE patterns most probably reflect varying degrees of partial melting for SKS lavas. The nearly constant HREE abundances are probably related to garnet in the source for these lavas (e.g. Lanphere & Frey, 1987). Patterns for the weakly alkalic lavas cross the patterns for some tholeiites at Nd; the pattern for sample KS2 crosses all of the patterns. The crossing REE patterns indicate distinct sources for many SKS lavas, especially the alkalic lavas. The vertical axis is linear rather than log scale to better show small-scale features. Symbols are as in Fig. 7. SKS data are from Table 3. The 2σ error bars are within the size of the symbol. Yellow fields for Kaua`i and Kōloa lavas are from Garcia *et al.* (2010).

Ka`ena deep-water (2800–3460 m) flat-topped cones just east of the SKS (20–35 vol. %; Greene *et al.*, 2010). The *in situ* occurrence of highly vesicular Hawaiian lavas in deep water opens the possibility that some of the highly vesicular SKS lavas (>20 vol. %) from dives 297 and 252 may not be landslide debris from Kaua`i, especially samples collected from cone-like features (e.g. dive 297, cones B and C at depths ~3500 m). In the next section, the geochemistry of these lavas is compared with that of other SKS tholeiitic lavas to determine whether there are significant differences based on sample location (cone vs other area) and vesicularity.

Geochemical variations

Tholeiitic lavas from SKS overlap in composition with those from the adjacent Ni`ihau and Kaua`i volcanoes (Figs 8–11). This overlap makes it difficult to distinguish using geochemistry rocks that might have been transported via landslides from those erupted in place. It is interesting to note that the isotopic variations are smaller for SKS than those for Kaua`i (Fig. 12), despite the wider areal coverage for SKS samples compared with the size of Kaua`i. Two distinct age groups are recognized for SKS tholeiites (5·4–4·8 vs 4·4–3·9 Ma; Ito *et al.*, 2013). Weakly vesicular rocks were found in both age groups, whereas the strongly vesicular lavas (>20 vol. %) were limited to the younger group (Fig. 4). No clear difference in geochemistry is seen between the older and younger SKS tholeiitic lavas (Tables 2–4). Likewise, no geochemical distinction was noted for the strongly vesicular samples compared with the weakly vesicular samples (e.g. Zr/Nb, 10·4–13·3 vs 10·7–13·3; $^{206}Pb/^{204}Pb$, 18·14–18·24 vs 18·13–18·38; ε_{Nd}, 5·8–6·6 vs 6·0–7·0; Tables 2–4). Samples from cones vs other areas also overlap geochemically (e.g. Zr/Nb, 10·4–13·3 vs 10·1–13·3) with the samples not from cones showing less isotopic variation ($^{206}Pb/^{204}Pb$, 18·13–18·38 vs 18·16–18·25; ε_{Nd}, 5·8–6·8 vs 6·2–6·8; Tables 2–4). Thus, no geochemical distinction was found for recognizing possible landslide rocks within the SKS sample suite. It is possible that none of the collected samples were derived from landslides but we cannot confirm nor exclude this possibility.

The similarity in geochemistry and isotopic composition for tholeiitic lavas from the SKS, Kaua`i, Ni`ihau and Wai`anae volcanoes indicates that the Hawaiian mantle plume source was well mixed on a broad scale when these volcanoes formed at 3–6 Ma (Fig. 13). This well-mixed source for the northern Hawaiian Island volcanoes contrasts strongly with the well-documented bilateral asymmetry that is observed for southern Hawaiian Island volcanoes (Moloka`i to Hawai`i, 0–2·5 Ma; e.g. Abouchami *et al.*, 2005; Jackson *et al.*, 2012).

Table 4: Pb, Sr, Nd and Hf isotope ratios for SKS rocks

Sample	$^{206}Pb/^{204}Pb$	± 2σ	$^{207}Pb/^{204}Pb$	± 2σ	$^{208}Pb/^{204}Pb$	± 2σ	$^{208}Pb^*/^{206}Pb^*$	$^{87}Sr/^{86}Sr$	± 2σ	$^{143}Nd/^{144}Nd$	± 2σ	ε_{Nd}	$^{176}Hf/^{177}Hf$	± 2σ	ε_{Hf}
Tholeiites															
252-04	18·1602	0·0007	15·4531	0·0016	37·9056	0·0018	0·9521	0·703692	0·000007	0·512970	0·000009	6·22	0·283057	0·000004	10·09
252-10	18·1952	0·0007	15·4582	0·0006	37·9288	0·0015	0·9510	0·703693	0·000006	0·512978	0·000008	6·63	0·283088	0·000004	11·17
297-04	18·2386	0·0005	15·4593	0·0005	37·9417	0·0012	0·9478	0·703656	0·000007	0·512996	0·000007	6·98	0·283099	0·000007	11·57
297-07	18·1892	0·0008	15·4578	0·0007	37·9290	0·0020	0·9517	0·703718	0·000007	0·512976	0·000007	6·60	0·283083	0·000005	11·00
297-07 (rep)	18·1895	0·0008	15·4586	0·0007	37·9335	0·0020	0·9521								
297-11	18·1602	0·0007	15·4549	0·0007	37·9625	0·0017	0·9586	0·703746	0·000009	0·512937	0·000008	5·84	0·283065	0·000006	10·38
297-18	18·1425	0·0007	15·4549	0·0007	37·8959	0·0015	0·9530	0·703710	0·000008	0·512961	0·000008	6·29	0·283083	0·000007	10·99
297-26	18·1444	0·0008	15·4560	0·0008	37·8945	0·0021	0·9526	0·703650	0·000007	0·512945	0·000008	5·99	0·283087	0·000007	11·13
297-26 (rep)	18·1468	0·0006	15·4585	0·0006	37·9011	0·0015	0·9531						0·283067	0·000006	10·43
298-07	18·3796	0·0009	15·4674	0·0008	38·0240	0·0022	0·9422	0·703589	0·000008	0·512987	0·000008	6·81	0·283109	0·000005	11·92
298-07 (rep)										0·512998	0·000006	7·02			
298-20	18·2867	0·0007	15·4593	0·0005	37·9587	0·0015	0·9447	0·703600	0·000007	0·512985	0·000008	6·77	0·283093	0·000006	11·36
298-20 (rep)													0·283094	0·000005	11·39
299-04	18·2408	0·0011	15·4618	0·0014	37·9640	0·0034	0·9501	0·703654	0·000007	0·512982	0·000008	6·71	0·283102	0·000008	11·66
299-20	18·2521	0·0011	15·4634	0·0007	37·9580	0·0010	0·9482	0·703724	0·000007	0·512974	0·000007	6·54	0·283067	0·000005	10·42
299-23	18·1881	0·0007	15·4564	0·0007	37·8955	0·0016	0·9480	0·703600	0·000009	0·512990	0·000008	6·86	0·283085	0·000007	11·06
299-29	18·1805	0·0008	15·4522	0·0007	37·9312	0·0018	0·9529	0·703725	0·000009	0·512957	0·000014	6·22	0·283073	0·000008	10·65
299-29 (rep)	18·1830	0·0008	15·4550	0·0007	37·9397	0·0019	0·9535						0·283069	0·000006	10·52
299-33	18·2011	0·0007	15·4592	0·0006	37·9401	0·0017	0·9517	0·703686	0·000007	0·512978	0·000007	6·63	0·283080	0·000005	10·90
KS1-13	18·1323	0·0006	15·4493	0·0006	37·8649	0·0017	0·9505	0·703722	0·000008	0·512946	0·000020	6·01			
KS1-13 (dup)	18·1333	0·0006	15·4494	0·0006	37·8659	0·0015	0·9506	0·703700	0·000007	0·512957	0·000006	6·22			
KS3-3	18·1925	0·0007	15·4547	0·0007	37·9402	0·0017	0·9526	0·703735	0·000007	0·512959	0·000006	6·01	0·283061	0·000005	10·23
Alkalic basalts															
KS-2	18·2792	0·0015	15·4542	0·0016	38·0152	0·0034	0·9517	0·703216	0·000008	0·513023	0·000007	6·25	0·283078	0·000005	10·81
297-20	18·0967	0·0017	15·4614	0·0014	37·7848	0·0036	0·9453	0·703312	0·000007	0·513031	0·000005	7·66	0·283180	0·000005	14·42
297-23	18·0807	0·0010	15·4571	0·0008	37·7702	0·0019	0·9454	0·703307	0·000007	0·513032	0·000005	7·69	0·283180	0·000009	14·44
297-23 (dup)	18·0816	0·0006	15·4586	0·0006	37·7737	0·0015	0·9456	0·703312	0·000008	0·513033	0·000005	7·70	0·283177	0·000008	14·33

Samples were analyzed for Pb and Hf using the Nu Plasma Instruments MC-ICP-MS system and for Sr using the Finnigan TRITON TIMS system. Nd analyzed by MC-ICP-MS; sample KS1-13 analyzed using TRITON TIMS. CHUR values used for calculation of ε_{Nd} are $^{143}Nd/^{144}Nd = 0{\cdot}512638$ and for ε_{Hf} $^{176}Hf/^{177}Hf = 0{\cdot}282772$ [DePaolo & Wasserburg (1976) and Blichert-Toft & Albarède (1997), respectively]. Duplicate refers to independent sample processing, whereas replicate analysis refers to repeated measurement of the same solution on the MC-ICP-MS system.

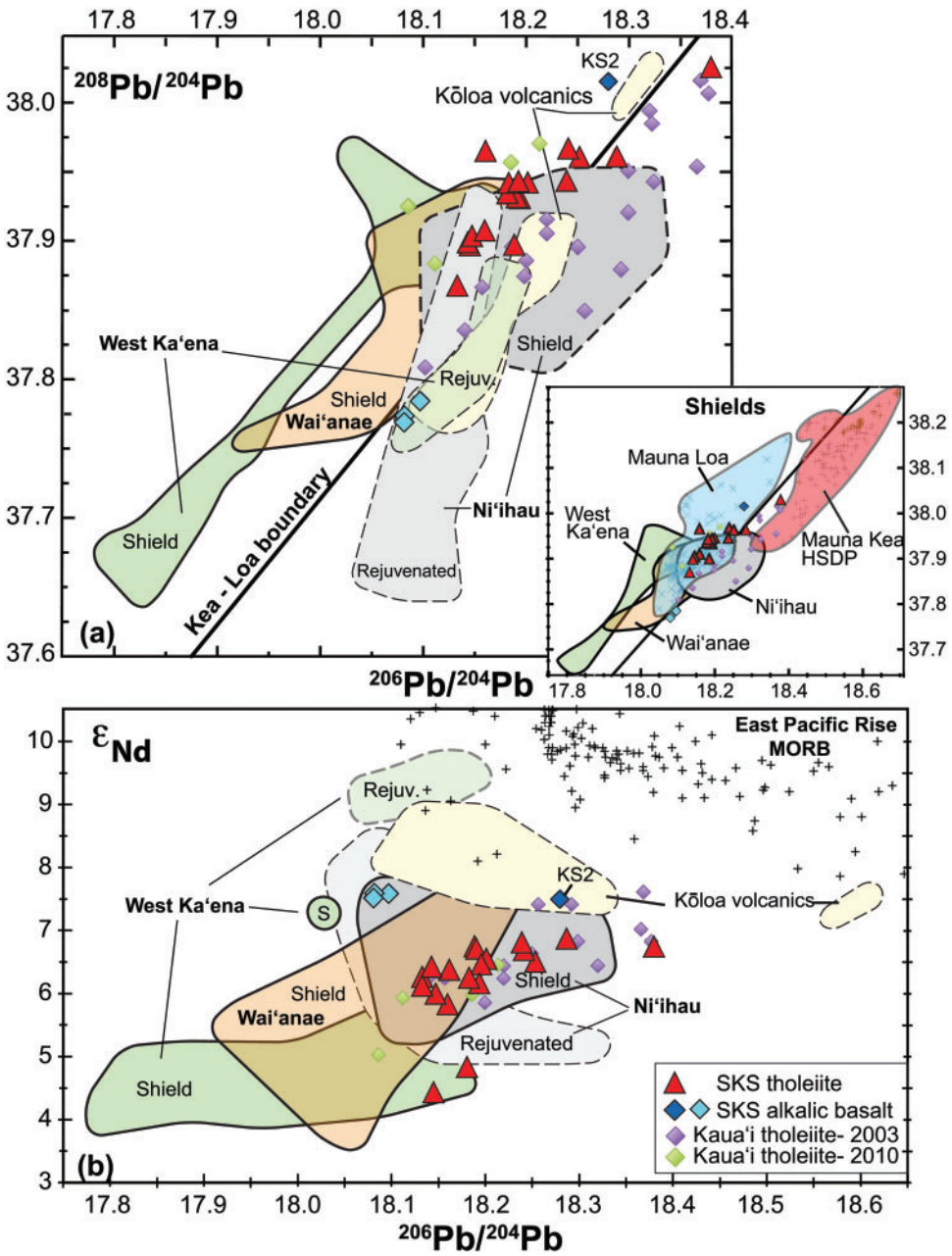

Fig. 11. Pb and Nd isotope variations in SKS lavas. (a) $^{206}Pb/^{204}Pb$ vs $^{208}Pb/^{204}Pb$; (b) $^{206}Pb/^{204}Pb$ vs ε_{Nd}. Inset plot: $^{206}Pb/^{204}Pb$ vs $^{208}Pb/^{204}Pb$ for lavas from northern Hawaiian Island volcanoes and Mauna Kea (HSDP, shield only; red field) and Mauna Loa (blue field) volcanoes. The remarkable overlap of the SKS tholeiitic lavas with the fields for other northern Hawaiian shield volcanoes should be noted. SKS data are from Table 4. SKS alkalic lavas are similar to rejuvenated lavas from other northern Hawaiian volcanoes (dashed fields). Symbols, fields and data sources as in Fig. 7, except Kaua`i tholeiites, 2003 (Mukhopadhyay *et al.*, 2003); Kaua`i tholeiites, 2010 (Garcia *et al.*, 2010) and EPR MORB (+) (Niu *et al.*, 1999; Regelous *et al.*, 1999; Castillo *et al.*, 2000), and Mauna Loa and Mauna Kea (Weis *et al.*, 2011; Nobre Silva *et al.*, 2013). The 2σ error bars are within the size of the symbol.

REGIONAL AGE VARIATIONS FOR SHIELD AND REJUVENATED VOLCANISM

There is substantial overlap in the ages of lavas from northern Hawaiian Island volcanoes (Wai`anae to Ni`ihau), a distance of 220 km along the Hawaiian Chain (Fig. 13). These ages indicate that coeval shield stage volcanism was widespread for this portion of the Hawaiian Islands. There are complications in interpreting the available ages for northern Hawaiian Island lavas, for the following reasons: (1) most of the ages were determined by K–Ar rather than the $^{40}Ar/^{39}Ar$ methods (except for eight from West Ka`ena and 16 from SKS); ages determined by $^{40}Ar/^{39}Ar$ are preferable for the older shield lavas because of their low K content and the mobility of K during low-temperature alteration; (2) the ages for shield lavas represent only the youngest phase of volcanism owing to limited exposures on Hawaiian volcanoes (only 10–20% of overall shield

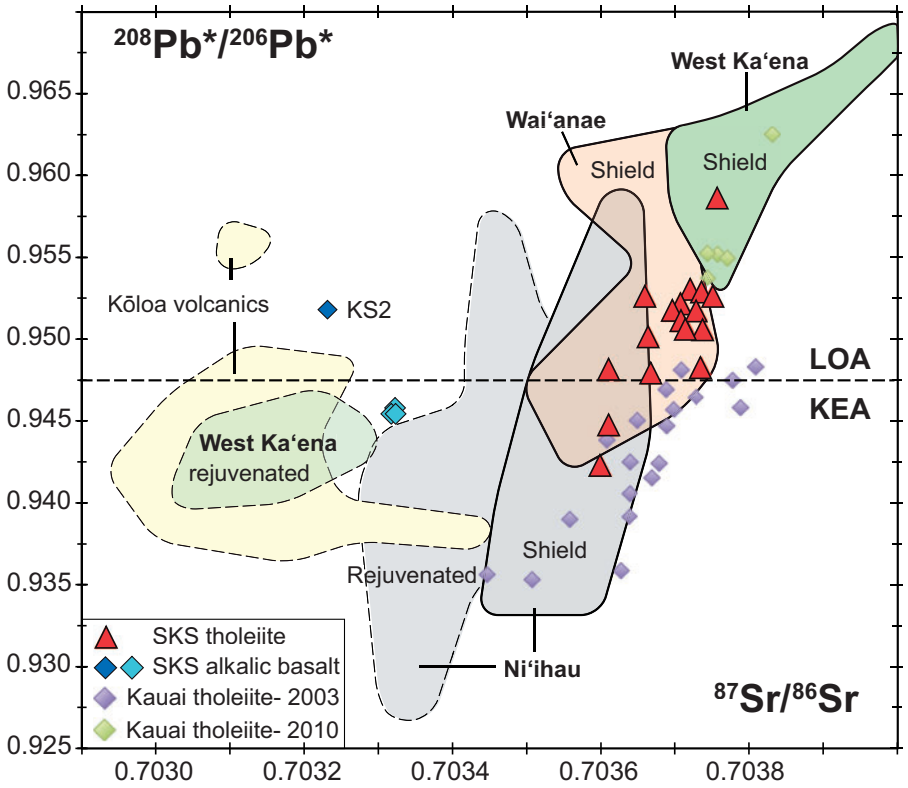

Fig. 12. Variation of $^{87}Sr/^{86}Sr$ vs $^{208}Pb^*/^{206}Pb^*$ for SKS lavas. The dashed Kea–Loa line is from Weis *et al.* (2011). Most of the SKS lavas, especially the tholeiites, plot in the Loa field, which is a common feature of shield lavas from other northern Hawaiian Island volcanoes. SKS data are from Table 4. Symbols, fields and data sources for other samples are as in Figs 7 and 11. The 2σ error bars are within the size of the symbol.

volcanism exposed); (3) erosion has removed significant parts of Ni`ihau; (4) the submarine volcanoes (SKS and West Ka`ena) are not well sampled. Despite these complications, the overlap in lava ages for these five widely spaced volcanoes is striking (Fig. 13).

One approach to examining the overlap in ages for the northern Hawaiian volcanoes is to focus on the youngest ages for tholeiitic rocks, which may represent the final stage of shield growth. The ages for samples from the closely spaced Kaua`i, SKS and West Ka`ena volcanoes (spanning only ~60 km along the Hawaiian Chain) show a decrease to the SE as expected from the overall age evolution on the archipelago. The youngest tholeiite age from West Ka`ena (2·85 ± 0·54 Ma, a K–Ar date with a large analytical error) appears to be anomalously young compared with those for nearby shields (Fig. 13). If this sample is excluded, the range in age for these three volcanoes is 0·6 Myr, which translates to an apparent rate for cessation of shield volcanism of ~100 km Ma^{-1} (Fig. 13). This value is identical to estimates for the rate of propagation of the southern part of the Hawaiian Chain (100 ± 10 km Ma^{-1}; Garcia *et al.*, 1987; Wessel & Kroenke, 2007) and the rate estimated for death of shields to the SE of Wai`anae to Kaho`olawe (~105 km Ma^{-1}; Sherrod *et al.*, 2007*b*). If the ages for the end of volcanism on Wai`anae and Ni`ihau volcanoes are included, there is a time span of only 1·2 Myr over a distance of ~220 km along the chain, producing a rate of 183 km Ma^{-1} for the end of shield volcanism. The ages of Wai`anae volcanism are well constrained by field work and paleomagnetic data (Sherrod *et al.*, 2007*b*). Thus, the mostly likely explanation for the apparent rapid rate of shield death for the northern Hawaiian Island shields is that the age for end of volcanism on Ni`ihau is too young, perhaps by 0·4–0·5 Myr. Sherrod *et al.* (2007*b*) recognized that the conventional K–Ar ages for Ni`ihau span too long a time period for the 400 m section of exposed lavas and noted that the youngest age has a large error (± 0·45 Myr). If this anomalous age is excluded, the time span for the five volcanoes is 1·65 Myr and the rate for the end of shield volcanism becomes ~135 km Ma^{-1}, which is much closer to the average propagation rate for the Hawaiian Islands over the last 6 Myr (100 ± 10 km Ma^{-1}; Garcia *et al.*, 1987; Wessel & Kroenke, 2007).

Another notable feature in the age data is the overlap for tholeiites from the five northern Hawaiian volcanoes (Fig. 13). These ages represent only the upper parts of these volcanoes. It is likely that volcanism at these volcanoes extended to earlier times, perhaps by at least 0·5 Myr based on estimates for the duration of shield volcanism (e.g. 1·5 Myr; Garcia *et al.*, 2006). Therefore, simultaneous shield volcanism probably occurred on the five northern Hawaiian Island shield volcanoes at 4·5–5 Ma. In comparison, tholeiitic volcanism on the southern Hawaiian Island volcanoes overlapped at ~1 Ma for only

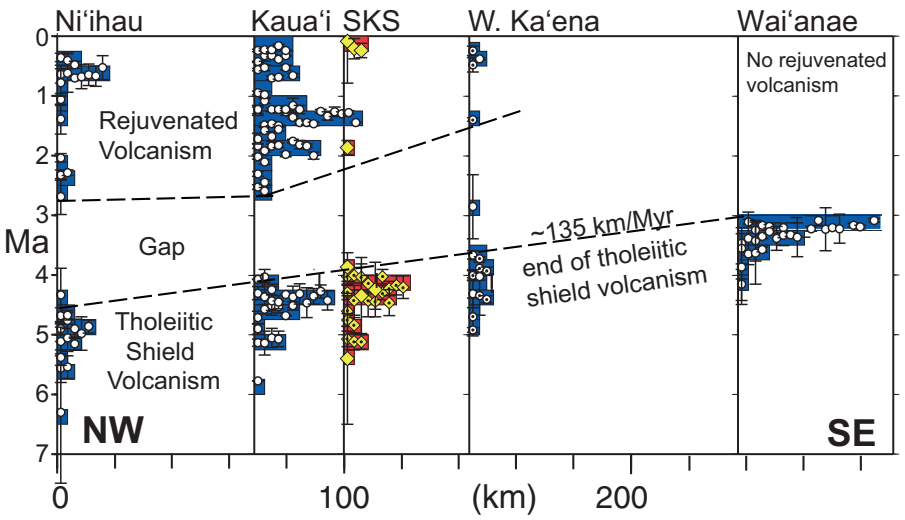

Fig. 13. Histograms of radiometric ages (Ma) for SKS and neighboring volcanoes (divided into 0·25 Ma age bins on the vertical axis). The squares represent the number of samples of a particular age, in red for SKS lavas and blue for other volcanoes. Each histogram is positioned horizontally according to the distance of the volcano from Kīlauea caldera, projected onto the trajectory of absolute Pacific Plate motion, HS3-Nuvel 1A (Gripp & Gordon, 2001). The 2σ error bars are given (if available) for each age. For SKS and W. Ka`ena samples, black dots designate $^{40}Ar/^{39}Ar$ ages; other SKS and W. Ka`ena ages are by the unspiked K–Ar method. Ages for Ni`ihau, Kaua`i and Wai`anae lavas were determined by conventional K–Ar methods. Data sources: Kaua`i from McDougall (1964, 1979), Clague & Dalrymple (1988) and Garcia *et al.*, 2010); W. Ka`ena from Greene *et al.* (2010); Ni`ihau and Wai`anae from Sherrod *et al.* (2007*b*).

~110 km on the Island of Hawai`i (Lipman & Calvert, 2013) and across the Maui Nui complex (e.g. Sherrod *et al.*, 2007*b*). However, these volcanoes are poorly exposed, so there may be greater overlap.

Rejuvenated volcanism in the northern Hawaiian Island region is widespread and long-lived (≥2 Myr for Ni`ihau, SKS and Kaua`i; Fig. 13). Among the southern Hawaiian Islands, only three of seven extinct Hawaiian Island shield volcanoes have experienced rejuvenated volcanism and, where present, it is localized and short-lived (e.g. three vents on East Moloka`i and four on West Maui; Sherrod *et al.*, 2007*a*). Ko`olau volcano is the exception with ~40 vents formed over ~0·7 Myr (Ozawa *et al.*, 2005), but this duration is still much shorter than that in the northern Hawaiian Islands. Another key feature is the simultaneous occurrence of rejuvenated volcanism from ~0·3 to 0·6 Ma along a 400 km segment of the Hawaiian Islands (Maui to Ni`ihau; Garcia *et al.*, 2010). This swath of coeval rejuvenated volcanism is wider than the predictions of the flexural uplift melting model (175–225 km; Bianco *et al.*, 2005) and the secondary melting model (200–250 km; Ribe & Christensen, 1999). The interaction of the Hawaiian plume with small-scale convection within the Pacific lithosphere and the presence of pyroxenite in the source are thought to enhance the volume and extend the duration of rejuvenated volcanism along the Hawaiian Chain (Ballmer *et al.*, 2011). The potential role of pyroxenite in the source of SKS lavas is examined in the next section.

PYROXENITE IN THE SOURCE FOR SKS LAVAS

Pyroxenite is considered an important source component for Hawaiian tholeiitic shield lavas based on whole-rock major elements and olivine composition (e.g. Hauri, 1996; Sobolev *et al.*, 2007; Jackson *et al.*, 2012). Hawaiian rejuvenated lavas are also thought to have a substantial pyroxenite component based on the relatively high $^{187}Os/^{188}Os$ isotope values reported for some rejuvenated lavas from Kaua`i and O'ahu (Lassiter *et al.*, 2000). Numerical modeling of melting within the Hawaiian plume has predicted a marked temporal variation in the pyroxenite component (Ballmer *et al.*, 2011). The wide range in ages for SKS tholeiitic and alkalic lavas (~1·5 and 1·8 Myr respectively) makes them valuable for evaluating the pyroxenite temporal variation model. We use two methods for estimating the pyroxenite component in melts for SKS lavas; olivine composition and trace elements (Gurenko *et al.*, 2010; Pietruszka *et al.*, 2013).

The composition of olivine in oceanic island lavas has been used to infer source lithology (pyroxenite vs peridotite; e.g. Hawai`i, Canaries, Azores, Reunion; Sobolev *et al.*, 2007; Gurenko *et al.*, 2009, 2010). Previous estimates of the amount of pyroxenite component in melts for lavas from Hawaiian shield volcanoes based on olivine chemistry range from 42% for Lō`ihi to 88% for Ko`olau, with typical values of 60–75% (Sobolev *et al.*, 2007). To estimate the weight fraction of pyroxenite-derived melt (X_{px}) in SKS lavas, we used the equation of Gurenko *et al.* (2010),

$$X_{px} = 6 \cdot 705E^{-04} \times (Ni \times FeO/MgO) - 1 \cdot 332E^{-02} \times (Mn/FeO) + 1 \cdot 5215 \quad (1)$$

where elemental concentrations of Ni and Mn are given in ppm, and concentrations of FeO and MgO in wt %. High-precision analyses were made for these

calculations using high beam current (200 nA) and voltage (20 kV), and long counting times (100 s for Ni, Ca, Mg and Si, and 60 s for Mn and Fe) using large crystals for Ni, Ca and Mn. These conditions resulted in 2σ errors that are <0·03 wt % for SiO_2, MgO and FeO and <0·01 wt % for CaO, MnO and NiO based on replicate analyses of the Smithsonian San Carlos Olivine standard. Euhedral olivine phenocrysts from eight SKS lavas (five tholeiitic and three alkalic lavas) that span the entire sampled age range of SKS and each rock group were analyzed using these methods.

The olivine results for the SKS lavas indicate elevated X_{px} components (Fig. 14; for single olivine results see Supplementary Data Electronic Appendix 4). The five tholeiitic samples have high average X_{px} values ranging from 68 to 89%, the highest value reported for Hawaiian lavas. The alkalic lavas have somewhat lower average X_{px} values (38, 50, 65%; Fig. 14). These are the first reported values for Hawaiian rejuvenated lavas. Measurements for some samples vary widely (20–35% for tholeiites, even if the most extreme values are excluded; Fig. 14). The large variation in X_{px} for SKS olivines reflects their wide range in MnO/FeO. The large variation in X_{px} does not correlate with Fo% or Ni content (see Supplementary Data Electronic Appendix 4). For example, the alkalic samples have a narrow range in Fo that plots near or in the equilibrium field (Fig. 5) but a large range in X_{px}. The tholeiitic lavas show larger ranges in Fo content (Appendix 4). If only the higher forsterite values are used for each sample, there is no significant difference in the calculated X_{px} value. For example, sample 299-41 has an Fo range of 82–88% and X_{px} range of 71–82. Using only the Fo 85–88 olivines results in no change in the X_{px} range and only a slight shift in the average X_{px} (from 77 to 78). Values of X_{px} do correlate positively with Ni content for the alkalic lavas, which have lower X_{px} and Ni values than the tholeiites (Fig. 3; Supplementary Data Electronic Appendix 4). The wide range in X_{px} for single samples is not related to the presence of xenocrysts because only euhedral, undeformed olivines were analyzed.

Broad correlations of X_{px} values with ε_{Nd} and radiogenic Pb isotope ratios are found in SKS lavas ($R^2 = 0{\cdot}79$; Supplementary Data Electronic Appendix 5). These correlations improve ($R^2 = 0{\cdot}91$) if the basanite lava KS2 (dark blue diamond in Appendix 5) is not included. The basanite represents a very low degree of partial melting based on its high incompatible element concentrations (Figs 9 and 10). Thus, this sample may be less representative of the two main source components in most SKS lavas. No correlation was found for X_{px} values and Sr isotope ratios for SKS samples (Table 4; Supplementary Data Electronic Appendix 4). No other study of Hawaiian lavas has measured isotopes and determined X_{px} values for the same samples. However, studies of some Atlantic oceanic island lavas have found rough correlations in the X_{px} values with Pb, Sr and Nd isotopes (e.g. $R^2 = 0{\cdot}52$–$0{\cdot}61$ for Madeira lavas; Gurenko *et al.*, 2013). The SKS lavas show the same trends of X_{px} with isotopes of Pb (positive) and ε_{Nd} (negative) as lavas from Madeira (Supplementary Data Electronic Appendix 5; Gurenko *et al.*, 2013). The pyroxenitic source component in the Madeira lavas was

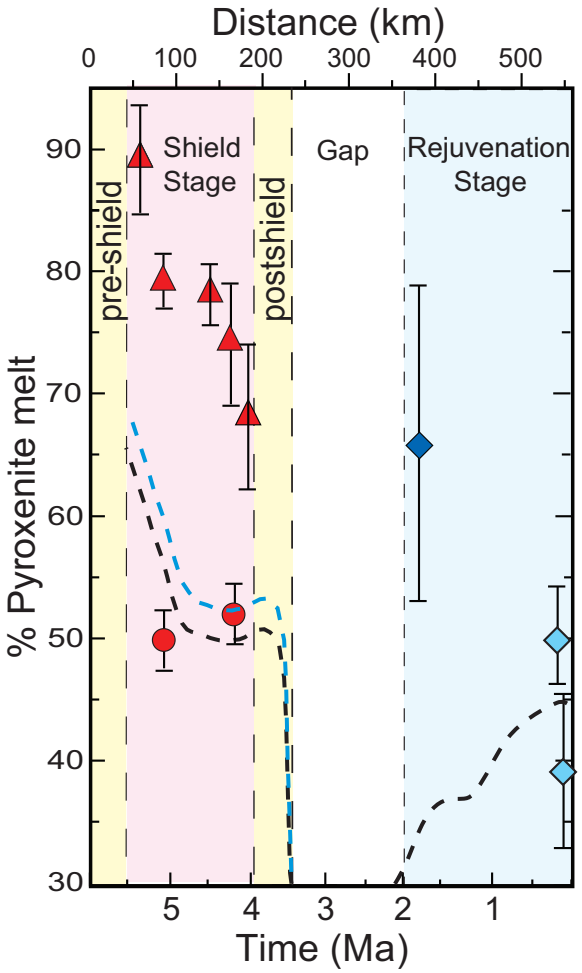

Fig. 14. Pyroxenite melt contribution (%) vs time and distance from Kīlauea for SKS lavas compared with estimates for an average Hawaiian volcano based on numerical modeling by Ballmer *et al.* (2011). Mean pyroxenite component (1σ shown by error bars) for eight dated SKS lavas based high-precision olivine analyses for tholeiites (red triangles), and alkalic lavas (blue diamonds; data in Supplementary Electronic Appendix 4) calculated using the equation of Gurenko *et al.* (2010) (see text for details). Mean solutions for the per cent pyroxenite melt component using the incompatible element method (Pietruszka *et al.*, 2013) are plotted as red circles for the two distinct SKS tholeiite age groups; older (4·8–5·1 Ma) and younger (4·0–4·3 Ma). The dashed black (average) and blue (Loa trend) curves show predictions of the temporal variation in the amount of pyroxenite in Hawaiian magmas based on a geodynamic model simulating the interaction of the Hawaiian plume with small-scale convection rolls in the 90 Ma Pacific oceanic lithosphere (Ballmer *et al.*, 2011). The curves for the shield stage show a temporal decrease in the pyroxenite component, which is consistent with the results for olivine. However, the absolute amount of the pyroxenite component inferred from the olivine data is much greater than predicted by numerical modeling (dashed curves); the latter is comparable with values calculated by the trace element method (red circles). The rejuvenated lavas show a temporal decrease in pyroxenite component based on the olivine method in contrast to the model trend (dashed curve).

related to recycled oceanic crust (Gurenko *et al.*, 2013). For Hawaiian lavas, high radiogenic Pb lavas (high X_{px} component in SKS lavas; Supplementary Data Electronic Appendix 5) are a characteristic of the Loa source component, which is thought to be derived from a large, low-shear-velocity province in the lower mantle under Hawai`i (e.g. Weis *et al.*, 2011).

Incompatible trace element abundances provide an alternative approach for estimating the amount of recycled oceanic crust (mafic component) in the mantle source of the Hawaiian lavas. This modeling, identical to the approach described in detail by Pietruszka *et al.* (2013), assumes that the recycled oceanic crust is made of altered mid-ocean ridge basalt (MORB) and related fresh lower crustal gabbro that are embedded in a matrix of ambient Hawaiian depleted mantle peridotite. These two components of recycled oceanic crust are assumed to have been processed in an ancient subduction zone, such that the uppermost portion of the recycled crust (i.e. altered MORB) preferentially lost the more fluid-mobile elements (e.g. Rb, Ba, U and, to a lesser extent, Th and the LREE) as the slab was dehydrated, whereas the gabbroic component from the lowermost portion of the crust is assumed to have accumulated plagioclase (causing elevated Sr and Eu abundances) and remained nearly isochemical during subduction. The trace element abundances assumed for the two components of the recycled oceanic crust (prior to dehydration of the altered MORB) and the ambient Hawaiian depleted mantle are identical to the values listed by Pietruszka *et al.* (2013), which are based on the compositions of altered MORB and gabbros drilled from the oceanic crust. For the modeling, this recycled oceanic crust is mixed with ambient Hawaiian depleted peridotitic mantle, and the combination is partially melted to create the Hawaiian parental magma.

A batch melting process is assumed to occur in a lithologically mixed peridotite–eclogite source (e.g. Sobolev *et al.*, 2005), in which the eclogite reacts with the peridotite at a depth below the volcano's melting region to make a secondary pyroxenite (and an eclogite residue that no longer melts). As upwelling of the mantle continues, the leftover unreacted peridotite and the secondary pyroxenite melt and mix to create the parental magma, as described by Pietruszka *et al.* (2013). The model parameters (the extent of dehydration for the altered MORB, the amount of altered MORB and fresh lower crustal gabbro in the source, and the degree of partial melting for the peridotite and pyroxenite) were varied iteratively to match the mean compositions of three groups of SKS lavas: (1) older tholeiites, 5·4–4·8 Ma; (2) younger tholeiites, 4·0–4·3 Ma; (3) alkalic lavas. Single samples from each of these groups were normalized to 16 wt % MgO by addition of equilibrium olivine in small increments to create hypothetical parental magma compositions as described by Pietruszka *et al.* (2013), which were averaged for each age group (for compositions, see Table 5). Solutions were obtained for the tholeiitic groups but no acceptable solution was found for the alkalic lavas (i.e. the trace element abundances of the alkalic lavas could not be matched within analytical uncertainty). The modeling results indicate that the tholeiitic magmas can all be produced by similar degrees of partial melting (4% melting of the peridotite and 23–25% melting of the pyroxenite) of a source that contained 12–13% recycled altered MORB that was dehydrated by ~3% fluid loss combined with 1·5–2% recycled lower crustal gabbro (Table 5). This represents a total recycled oceanic crust component of ~13–15% in the source. The amount of

Table 5: Summary of the trace element model results for SKS parent magmas

	Younger tholeiites (4·0–4·3 Ma)		Older tholeiites (4·8–5·1 Ma)	
	Parent melt (norm.)	Model residuals (% diff.)	Parent melt (norm.)	Model residuals (% diff.)
Rb	8·1	(1·0)	10·0	(–7·7)
Ba	9·9	(0·7)	10·9	(1·7)
Th	7·4	(8·2)	7·6	(18·6)
U	9·4	(5·9)	11·2	(–1·0)
Nb	13·1	(0·0)	14·4	(0·0)
La	12·9	(–8·0)	12·7	(2·7)
Ce	12·7	(–2·5)	12·9	(4·0)
Pr	11·3	(–1·1)	12·1	(–1·2)
Sr	12·4	(0·0)	13·0	(0·0)
Nd	11·1	(–4·7)	12·1	(–8·2)
Sm	9·4	(0·2)	10·0	(–2·4)
Zr	9·8	(–0·3)	11·5	(–13·4)
Eu	8·5	(–1·8)	8·9	(–4·3)
Gd	7·4	(–0·8)	8·0	(–6·4)
Tb	6·3	(1·4)	6·8	(–4·4)
Dy	5·7	(–3·7)	5·9	(–6·9)
Ho	4·6	(2·1)	4·7	(–0·6)
Y	4·3	(1·6)	4·2	(4·5)
Er	4·1	(2·5)	4·3	(–3·2)
Tm	3·2	(17·1)	3·6	(4·8)
Yb	3·3	(–1·7)	3·3	(–2·7)
Lu	3·1	(1·7)	3·0	(2·7)
Source materials				
Altered MORB (%)		12·7		11·8
Lower crustal gabbro (%)		2·1		1·5
Total oceanic crust (%)		14·8		13·3
Hawaiian depleted mantle (%)		85·2		86·7
Model parameters				
X_f (%)		3·0		3·1
F_{pd} (%)		4·2		3·9
F_{px} (%)		25·3		23·2
X_{px} (%)		53·4		49·9

The model of Pietruszka *et al.* (2013) was applied to average compositions for the younger (297–04, 297–18, 299–23, 252–04, and 252–10) and older (297–26, 298–20, 299–20, and 299–33) tholeiitic parental magmas. Single samples from each of these groups were normalized to 16 wt % MgO by addition of equilibrium olivine in small increments to create hypothetical parental magma compositions (parent melt norm.) as described by Pietruszka *et al.* (2013). The average of each MgO-normalized group [shown above, normalized to the primitive mantle values of Sun & McDonough (1989)] was modeled assuming a lithologically heterogeneous source (peridotite and a secondary pyroxenite; Sobolev *et al.*, 2005) to determine the amount of ancient, recycled ocean crust (both altered MORB and lower crustal gabbro) in the mantle source of the parental magmas. X_f is the extent of dehydration for the altered MORB, F_{pd} is the melt fraction for the peridotite source, F_{px} is the melt fraction for the pyroxenite source, and X_{px} is the fraction of melt from the pyroxenite source. The residuals (expressed as the per cent difference between the model result and the average parental magma composition) are shown for each element in parentheses.

melt derived from the pyroxenite source (X_{px}) for the two age groups of tholeiitic magmas is nearly identical, 50 and 53% (Table 5). These values are much lower than the estimates of pyroxenite component in the melt calculated from olivine compositions (Fig. 14). However, both methods indicate a significant (≥50%) component of pyroxenite in the magmas for SKS shield lavas.

The trace element modeling solutions for recycled oceanic crust components in the source for SKS magmas are comparable with those calculated for the source of Kīlauea lavas including those from the continuing Pu'u 'O'ō eruption (~12–13%) and its prehistoric Mauna Loa-like lavas (~14–16%), but are somewhat lower than those calculated for the source of recent Mauna Loa lavas (~17–21%; Pietruszka *et al.*, 2013). The similarity of the source lithologies for SKS and Kīlauea lavas is consistent with the comparable Sr and Nd isotopic compositions of the SKS and prehistoric Mauna Loa-like Kīlauea lavas (e.g. Marske *et al.*, 2007).

Hawaiian volcanoes display a remarkable temporal variation in melt flux (e.g. Garcia *et al.*, 2006). A recent geodynamic modeling study of the Hawaiian plume addressed the potential role of melting a mixed peridotite and pyroxenite source in controlling this temporal variation (Ballmer *et al.*, 2011). Their models predict that during the voluminous shield stage of volcanism, the percentage of pyroxenite in the melt (X_{px}) is initially high (~65%) and decreases with time to ~50% (Fig. 14). Following a hiatus of volcanism, low but increasing values of magma flux and X_{px} are predicted to occur during the rejuvenation stage (Fig. 14). The Ballmer *et al.* (2011) model indicates that initial melting during the rejuvenation stage was relatively shallow (125–135 km) involving depleted harzburgite stripped of its pyroxenite component. Later melting was deeper (135–150 km) involving increasing amounts of pyroxenite upwelling from the periphery of the mantle plume stem. This portion of the plume is thought to have largely bypassed the main melting zone and avoided depletion. The temporal increase in X_{px} was predicted to extend the duration of rejuvenated volcanism to ~3 Myr (Ballmer *et al.*, 2011).

The temporal decrease in X_{px} calculated from olivine analyses for SKS shield stage lavas is consistent with the trend predicted by the Ballmer *et al.* (2011) modeling (Fig. 14). The olivine X_{px} values, however, are higher than predicted by their geodynamic model, a difference that could be reduced if a greater proportion of pyroxenite were used in the source in the geodynamic model. In contrast, X_{px} values from the incompatible trace elements calculations are comparable with those predicted by the geodynamic model (Fig. 14), although the two models predict different extents of melting and assume different source compositions (~50% less pyroxenite in the source for the geodynamic model compared with the concentration of oceanic crust in the source for the trace-element model).

The minimum in magma flux predicted by the geodynamic model of Ballmer *et al.* (2011) is consistent with the ~1–2 Myr gap in volcanism that typically follows the shield stage on the Hawaiian Islands (Ozawa *et al.*, 2005; Garcia *et al.*, 2010) and the apparent ~2 Myr gap for SKS volcano (Fig. 13). The model prediction of a 3 Myr duration for rejuvenated volcanism is longer than the 2–2·5 Myr observed for northern Hawaiian shield volcanoes (SKS, Kaua`i, and Ni`ihau). However, the presence of young volcanism on SKS and Kaua`i (0·1–0·2 Ma; Garcia *et al.*, 2010; Ito *et al.*, 2013) and the episodic nature of Hawaiian rejuvenated volcanism (Ozawa *et al.*, 2005) support the geodynamic model prediction. Thus, volcanism in these areas may occur again.

LOA SOURCE COMPONENT FOR NORTHERN HAWAIIAN ISLAND VOLCANOES

Bilateral isotopic asymmetry is observed for lavas from many oceanic island chains (e.g. Hawai`i, Samoa, Marquesas; Abouchami *et al.*, 2005; Huang *et al.*, 2011; Weis *et al.*, 2011; Chauvel *et al.*, 2012; Jackson *et al.*, 2014). The southern Hawaiian Island lavas (Hawai`i to O'ahu, 0–2·5 Ma) display the classic example of bilateral Pb isotopic asymmetry (Tatsumoto, 1987; Abouchami *et al.*, 2005; Hanano *et al.*, 2010). The asymmetry is seen between two volcano subchains: the southwestern 'Loa' chain has $^{208}Pb^*/^{206}Pb^* > 0.9475$ and includes Mauna Loa, and the northeastern 'Kea' chain has $^{208}Pb^*/^{206}Pb^* < 0.9475$ and includes Mauna Kea, both volcanoes being the tallest on the island of Hawai`i. It was thought that the two trends terminated at the Moloka`i fracture zone and that a single line could be drawn through the locations of the northern Hawaiian Island volcanoes, which supposedly had Kea-like Pb isotope compositions (Abouchami *et al.*, 2005; Tanaka *et al.*, 2008). However, the Kaua`i–Ni`ihau-Ka`ula lineament cannot be linked with the other Hawaiian volcanoes by a single line (Fig. 1) and recent studies have shown Loa-like isotopic Pb signatures for lavas north of O`ahu (W. Ka`ena and Kaua`i; Garcia *et al.*, 2010; Greene *et al.*, 2010; Weis *et al.*, 2011).

Kea-like $^{208}Pb^*/^{206}Pb^*$ compositions were found in only four of the 19 analyzed SKS lavas (two tholeiites and two weakly alkalic lavas; Fig. 12; Table 3). These Kea-like lavas are widely separated (dive 298, on the southern flank of the SKS and dive 297 on the NW flank) and range in age from 0·1 to 4·8 Ma (Table 4 and Supplementary Data Electronic Appendix 6). Thus, there is no apparent geographical or temporal correlation of the SKS Kea-like lavas. Most (14 of 16) SKS tholeiitic lavas and the basanite lava exhibit Loa-like radiogenic Pb ratios (Fig. 12), which is consistent with the volcano's geographical location on the west side of the Hawaiian Islands (e.g. Weis *et al.*, 2011). Many of the lavas from the adjacent Ni`ihau volcano, also on the west side of the Hawaiian Islands, have Loa-like Pb isotope ratios (Fig. 12). The presence of Loa-trend Pb isotope ratios in the older volcanic rocks from SKS

(5·1–5·4 Ma; Table 4) and Ni`ihau (~5·5 Ma; Cousens & Clague, in preparation) extends the regional extent of the Loa, enriched Hawaiian mantle source component to include the entire main Hawaiian Island segment (~600 km long) of the Hawaiian Ridge.

Kaua`i shield and rejuvenated lavas show Loa radiogenic Pb isotope ratios (Garcia *et al.*, 2010). This observation deviates from the general Loa–Kea geographical distinction, because Kaua`i lies on the east side of the main axis of the Hawaiian chain (Fig. 1). Some variation in radiogenic Pb isotope ratios is also observed at other shield volcanoes on both sides of the Hawaiian Islands, although Kea-like Pb isotopic signatures are significantly more common on the east side and Loa-like values on the west side (e.g. Weis *et al.*, 2011; Xu *et al.*, 2014). The common occurrence of Loa-like Pb isotope values among lavas from all of the northern Hawaiian volcanoes (SKS, Kaua`i, Ni`ihau and Wai`anae; Fig. 12) and Ko`olau indicates that this source component is ubiquitous for the northern Hawaiian Island shield volcanoes, unlike for the southern Hawaiian volcanoes (e.g. Weis *et al.*, 2011). The prevalence and broad occurrence of the Loa component in the northern part of the Hawaiian Islands coincides in time and space with the beginning of a dramatic increase (300%) in magma flux during the formation of the Hawaiian Islands (Fig. 1). If the increase in magma flux is related to the emergence of the Loa source component in the Hawaiian mantle plume, these observations provide evidence for a fundamental change in its internal structure. This change included not only the potential emergence of the Loa component at ~6 Ma during the formation of the northern Hawaiian Islands but also the later (at ~2 Ma) segregation of the Loa and Kea components into filaments (e.g. Farnetani & Hofmann, 2010; Weis *et al.*, 2011) on the west and east sides of the plume as the island of Moloka`i formed. Alternatively, it has been proposed that the Loa and Kea components are well mixed within the plume and that the two trends reflect higher temperature melting at the core of the plume for the Kea side and lower temperature on the plume periphery for the Loa side (e.g. Ren *et al.*, 2005; Xu *et al.*, 2014). This model would require a shift in the melting regions of the plume between the northern and southern Hawaiian Islands. This zoned melting model conflicts with estimates of per cent melting based on trace elements, which indicate that Loa lavas represent higher degrees of melting than the Kea lavas (e.g. Norman & Garcia, 1999).

Resolving the longevity of the Loa component in the Hawaiian plume and the role of this source component in explaining the dramatic increase in the eruptive volume along the Hawaiian Ridge (Fig. 1) requires more sampling north of the Hawaiian Islands.

CONCLUSIONS

The SKS is a large (110 km × 80 km) submarine shield volcano with numerous small (<1 km wide) seamounts. The petrology and geochemistry of the SKS lavas were characterized in this study. Our results show the following.

1. Two geochemically distinct groups of rocks are present at SKS volcano: tholeiites and alkalic basalts. The majority of the samples are tholeiitic with ages of 3·9–5·4 Ma, which correspond to the shield stage of volcanism. About 10% of the analyzed samples are weakly to moderately alkaline basalts with much younger ages (0·1–1·9 Ma), which are related to the rejuvenated phase of SKS volcanism.
2. The age of SKS shield volcanism overlaps with ages for shield volcanism on other northern Hawaiian Island volcanoes (Wai`anae, West Ka`ena, Kaua`i and Ni`ihau). Thus, shield stage volcanism was simultaneous along ~220 km of the Hawaiian Chain compared with only ~110 km for the southern Hawaiian Islands. Coeval volcanism was even more widespread during the rejuvenation stage at 0·5 Ma, extending for 400 km from Ni`ihau to West Maui. This long span of coeval rejuvenated volcanism is much wider than predicted by the flexure (175–225 km) or secondary plume (200–250 km) melting models.
3. Tholeiitic SKS lavas range widely in their geochemistry and isotopic composition but are remarkably similar to coeval lavas from the shield stage of volcanism on Ni`ihau, Kaua`i and Wai`anae volcanoes. The geochemical similarity of tholeiitic lavas from the northern Hawaiian volcanoes makes it impossible to evaluate whether some of the rocks we recovered from SKS were derived from landslides of adjacent volcanoes. The similarity in composition for lavas from these volcanoes indicates that the heterogeneities within Hawaiian mantle plume source were well mixed when these volcanoes formed at 3–6 Ma.
4. Both the trace element and olivine methods for estimating the pyroxenite component in the parental melts of Hawaiian shield lavas indicate a major role for recycled oceanic crust (≥50%) in the source for SKS tholeiitic magmas. The temporal variation in pyroxenite component as inferred from olivine compositions in SKS tholeiitic lavas is consistent with the predictions of geodynamic models that simulate progressive depletion of more fusible pyroxenite veins followed by more extensive melting of peridotite. The amount of a recycled crustal component in the SKS tholeiites calculated using the trace element method is identical to calculated values for Kīlauea. These results are consistent with the similarity in Sr and Nd isotopic compositions for lavas from the two volcanoes. The presence of a significant pyroxenite component in the source for SKS rejuvenated lavas (40–65%) may have extended the duration (≥1·8 Myr) and volume of secondary volcanism for the northern Hawaiian Island volcanoes compared with other Hawaiian Island volcanoes, as suggested by the geodynamic model predictions.

5. The calculated pyroxenitic component in SKS lavas (based on the high-precision olivine analyses) shows a good correlation with Nd and radiogenic Pb isotope ratios for the shield and weakly alkalic lavas ($R^2 = 0{\cdot}91$). Similar correlations for the pyroxenitic component with isotopes were reported for lavas from Madeira volcano (positive trend for radiogenic Pb and negative for ε_{Nd}) but with lower R^2 values (0·61 and 0·52, respectively). The higher pyroxenite component in Hawaiian lavas is characteristic of the Loa source component, which is thought to be derived from a large, low-shear-velocity province in the lower mantle under Hawai`i.
6. Most (~80%) of the analyzed SKS samples have $^{208}Pb^*/^{206}Pb^*$ values $> 0{\cdot}9475$ indicating a Loa-like source. The presence of Loa-like Pb isotope ratios in rocks >5 Myr old from SKS and adjacent Ni`ihau volcanoes extends the duration of this enriched source component within the Hawaiian mantle plume. The dominance of Loa-like Pb isotope values for SKS rocks is consistent with the volcano's geographical location on the west side of the Hawaiian chain. Lavas from nearby Ni`ihau and Kaua`i shield volcanoes also commonly have Loa-like Pb isotope compositions, indicating that this component was common in the source for northern Hawaiian shield volcanoes. The prevalence and broad distribution of the Loa source component in the northern part of the Hawaiian Islands coincides in time and space with the start of a 300% increase in magma flux along the Hawaiian Ridge. Perhaps these two features are related and reflect a major change in the internal structure of the Hawaiian mantle plume.

ACKNOWLEDGEMENTS

We thank the Northern Hawaiian Islands Expedition science team (Dennis Geist, Terry Naumann, Chuck Blay, Diane Hanano, Inês Nobre Silva, Ashton Flinders, Claude Maerschalk, Brandon Christensen and Karen Harpp) for their amazing efforts during and after the expedition, the JASON team from Woods Hole Oceanographic Institution, and the Captain and crew of the University of Hawai`i R.V. *Kilo Moana* for retrieving the rocks and making the expedition safe. Thanks go to Diana Oettel for petrographic observations and many olivine analyses. Lindsay Spencer and Kyle Taniguchi are thanked for help with sample preparation, Michael Vollinger for sample washing and XRF analyses, Vivian Lai for assistance with the ICP-MS analyses, Bruno Kieffer for the Sr and Nd isotope analyses, Jane Barling and Alyssa Shiel for their assistance with the Pb and Hf isotopic analyses, and Maxim Ballmer for discussions on plume dynamics. We gratefully recognize constructive reviews by Brian Cousens, Matt Jackson and an anonymous reviewer, which led to improvements to this paper. This is SOEST contribution 9444.

FUNDING

This research was supported by the US National Science Foundation (grants EAR-0510482 to M.O.G. and G.I., EAR-1219955 and EAR-1347915 to M.O.G., and EAR-1141938 to G.I.).

SUPPLEMENTARY DATA

Supplementary data for this paper are available at *Journal of Petrology* online.

REFERENCES

Abouchami, W., Hofmann, A. W., Galer, S. J. G., Frey, F. A., Eisele, J. & Feigenson, M. (2005). Lead isotopes reveal bilateral asymmetry and vertical continuity in the Hawaiian mantle plume. *Nature* **434**, 851–856.

Armstrong, J. T. (1988). Quantitative analysis of silicate and oxide materials: Comparison of Monte Carlo, ZAF, and rho(pz) procedures. In: Newbury, D. E. (ed.) *Microbeam Analysis*. San Francisco, CA: San Francisco Press, pp. 239–246.

Ballmer, M. D., van Ito, G. Hunen, J. & Tackley, P. (2011). Spatial and temporal variability in Hawaiian hotspot volcanism induced by small-scale convection. *Nature Geoscience* **4**, 457–460.

Bianco, T. A., Ito, G., Becker, J. M. & Garcia, M. O. (2005). Secondary Hawaiian volcanism formed by flexural arch decompression. *Geochemistry,* Geophysics*, Geosystems* **6**, Q08009, doi:10.1029/2005GC000945.

Blichert-Toft, J. & Albarède, F. (1997). The Lu–Hf isotope geochemistry of chondrites and the evolution of the mantle–crust system. *Earth and Planetary Science Letters* **148**, 243–258.

Carpentier, M., Weis, D. & Chauvel, C. (2013). Large U loss during weathering of upper continental crust: The sedimentary record. *Chemical Geology* **340**, 91–104.

Castillo, P. R., Klein, E., Bender, J., Langmuir, C., Shirey, S., Batiza, R. & White, W. (2000). Petrology and Sr, Nd, and Pb isotope geochemistry of mid-ocean ridge basalt glasses from the 11°45′N to 15°00′N segment of the East Pacific Rise. *Geochemistry, Geophysics, Geosystems* **1**, 1011, doi:10.1029/1999GC000024.

Chauvel, C., Maury, R. C., Blais, S., Lewin, E., Guillou, H., Rossi, P. & Gutscher, M.-A. (2012). The size of plume heterogeneities constrained by Marquesas isotopic stripes. *Geochemistry, Geophysics, Geosystems* **13**, Q07005, doi:10.1029/2012GC004123.

Clague, D. A. & Dalrymple, G. B. (1988). Age and petrology of alkalic postshield and rejuvenated-stage lava from Kauai, Hawaii. *Contributions to Mineralogy and Petrology* **99**, 202–218.

Clague, D. A. & Frey, F. A. (1982). Petrology and trace element chemistry of the Honolulu volcanics, Oahu: Implication for the oceanic mantle below Hawaii. *Journal of Petrology* **23**, 447–504.

Clague, D. A., Moore, J. G., Dixon, J. E. & Friesen, W. B. (1995). Petrology of submarine lavas from Kilauea's Puna Ridge, Hawaii. *Journal of Petrology* **36**, 299–349.

Clague, D. A., Moore, J. G. & Reynolds, J. R. (2000). Formation of submarine flat topped volcanic cones in Hawaii. *Bulletin of Volcanology* **62**, 214–233.

Connelly, J. N., Ulfbeck, D. G., Thrane, K., Bizzarro, M. & Housh, T. (2006). A method for purifying Lu and Hf for analyses by

MC-ICP-MS using TODGA resin. *Chemical Geology* **233**, 126–136.

Coombs, M. L., Clague, D. A., Moore, G. F. & Cousens, B. L. (2004). Growth and collapse of Waianae Volcano, Hawaii, as revealed by exploration of its submarine flanks. *Geochemistry, Geophysics, Geosystems* **5** (Q08006), doi:10.1029/2004GC000717.

Davis, M. G., Garcia, M. O. & Wallace, P. (2003). Volatiles in glasses from Mauna Loa, Hawaii: Implications for magma degassing and contamination, and growth of Hawaiian volcanoes. *Contributions to Mineralogy and Petrology* **144**, 570–591.

DePaolo, D. J. & Wasserburg, G. J. (1976). Nd isotopic variations and petrogenetic models. *Geophysical Research Letters* **3**, 249–252.

Eggins, S. M., Woodhead, J. D., Kinsley, L. P. J., Mortimer, G. E., Sylvester, P., McCulloch, M. T., Hergt, J. & Handler, M. R. (1997). A simple method for the precise determination of $\geq$40 trace elements in geological samples by ICPMS using enriched isotope internal standardisation. *Chemical Geology* **134**, 311–326.

Farnetani, C. G. & Hofmann, A. W. (2010). Dynamics and internal structure of the Hawaiian plume. *Earth and Planetary Science Letters* **295**, 231–240.

Flinders, A. F., Ito, G. & Garcia, M. O. (2010). Gravity anomalies of the Northern Hawaiian Islands: Implications on the shield evolutions of Kauai and Niihau. *Journal of Geophysical Research* **115**, B08412, doi:08410.01029/02009JB006877.

Garcia, M. O. (1996). Petrography, olivine and glass chemistry of lavas from the Hawaii Scientific Drilling Project. *Journal of Geophysical Research* **101**, 11701–11713.

Garcia, M. O. (2002). Submarine picritic basalt from Ko`olau volcano, Hawai'i: Implications for parental magma composition and mantle source. In: Takahashi, E., Lipman, P. W., Garcia, M. O., Naka, J. & Aramaki, S. (eds) *Hawaiian Volcanoes. Deep Underwater Perspectives. American Geophysical Union, Geophysical Monograph* **128**, 391–402.

Garcia, M. O., Grooms, D. & Naughton, J. (1987). Petrology and geochronology of volcanic rocks from seamounts along and near the Hawaiian Ridge. *Lithos* **20**, 323–336.

Garcia, M. O., Foss, D. J. P., West, H. B. & Mahoney, J. J. (1995). Geochemical and isotopic evolution of Loihi volcano, Hawaii. *Journal of Petrology* **36**, 1647–1674.

Garcia, M. O., Caplan-Auerbach, J., De Carlo, E. H., Kurz, M. D. & Becker, N. (2006). Geology, geochemistry and earthquake history of Loihi seamount, Hawaii's youngest volcano. *Chemie der Erde* **66**, 81–108.

Garcia, M. O., Haskins, E. H., Stolper, E. M. & Baker, M. (2007). Stratigraphy of the Hawai`i Scientific Drilling Project core (HSDP2): Anatomy of a Hawaiian shield volcano. *Geochemistry, Geophysics, Geosystems* **8**, Q02G20, doi:10.1029/2006GC001379.

Garcia, M. O., Ito, G., Weis, D., et al. (2008). Widespread secondary volcanism around the northern Hawaiian Islands. *EOS Transactions, American Geophysical Union* **52**, 542–543.

Garcia, M. O., Swinnard, L., Weis, D., Greene, A. R., Tagami, T., Sano, H. & Gandy, C. E. (2010). Petrology, geochemistry and geochronology of Kauai lavas over 4·5 Myr: Implications for the origin of rejuvenated volcanism and the evolution of the Hawaiian Plume. *Journal of Petrology* **51**, 1507–1540.

Greene, A. R., Garcia, M. O., Weis, D., Ito, G., Kuga, M., Robinson, J. & Yamasaki, S. (2010). Low-productivity Hawaiian volcanism between Kauai and Oahu. *Geochemistry, Geophysics, Geosystems* **11**, Q0AC08, doi:10.1029/2010GC003233.

Gripp, A. E. & Gordon, R. G. (2001). Young tracks of hotspots and current plate velocities. *Geophysical Journal International* **150**, 321–361.

Gurenko, A. A., Sobolev, A. V., Hoernle, K., Hauff, F. & Schmincke, H.-U. (2009). Enriched, HIMU-type peridotite and depleted recycled pyroxenite in the Canary plume: a mixed-up mantle. *Earth and Planetary Science Letters* **277**, 514–524.

Gurenko, A. A., Hoernle, K. A., Sobolev, A. V., Hauff, F. & Schmincke, H.-U. (2010). Source components of the Gran Canaria (Canary Islands) shield stage magmas: evidence from olivine composition and Sr–Nd–Pb isotopes. *Contributions to Mineralogy and Petrology* **159**, 689–702.

Gurenko, A. A., Geldmacher, J., Hoernle, K. A. & Sobolev, A. V. (2013). A composite, isotopically-depleted peridotite and enriched pyroxenite source for Madeira magmas: Insights from olivine. *Lithos* **170–171**, 224–238.

Hanano, D., Weis, D., Scoates, J. S., Aciego, S. & DePaolo, D. J. (2010). Horizontal and vertical zoning of heterogeneities in the Hawaiian mantle plume from the geochemistry of consecutive postshield volcano pairs: Kohala–Mahukona and Mauna Kea–Hualalai. *Geochemistry, Geophysics, Geosystems* **11**, Q01004, doi:10.1029/2009GC002782.

Hauri, E. H. (1996). Major-element variability in the Hawaiian mantle plume. *Nature* **382**, 415–419.

Holcomb, R. T. & Robinson, J. E. (2004). Maps of the Hawaiian Islands Exclusive Economic Zone interpreted from GLORIA sidescan-sonar imagery. *US Geological Survey, Scientific Investigations Map* **2824**.

Huang, S., Hall, P. S. & Jackson, M. G. (2011). Geochemical zoning of volcanic chains associated with Pacific hotspots. *Nature Geoscience* **4**, 874–878.

Ito, G., Garcia, M. O., Smith, J. R., Taylor, B., Flinders, A., Jicha, B., Yamasaki, S., Weis, D., Swinnard, L. & Blay, C. (2013). A low relief shield volcano origin for the South Kaua`i Swell. *Geochemistry, Geophysics, Geosystems* **14**, 2328–2348.

Jackson, M. G., Weis, D. & Huang, S. (2012). Major element variations in Hawaiian shield lavas: Source features and perspectives from global ocean island basalt (OIB) systematics. *Geochemistry,Geophysics and Geosystems* **13**, Q09009, doi:10.1029/2012GC004268.

Jackson, M. G., Hart, S. R., Konter, J. G., Kurz, M. D., Blusztajn, J. & Farley, K. (2014). Helium and lead isotopes reveal the geochemical geometry of the Samoan plume. *Nature* **514**, 355–358.

Lanphere, M. A. & Frey, F. A. (1987). Geochemical evolution of Kohala Volcano, Hawaii. *Contributions to Mineralogy and Petrology* **95**, 100–113.

Lassiter, J. C., Hauri, E. H., Reiners, P. W. & Garcia, M. O. (2000). Generation of Hawaiian post-erosional lavas by melting of a mixed lherzolite/pyroxenite source. *Earth and Planetary Science Letters* **178**, 269–284.

Libourel, G. (1999). Systematics of calcium partitioning between olivine and silicate melt: implications for melt structure and calcium content of magmatic olivines. *Contributions to Mineralogy and Petrology* **136**, 63–80.

Lipman, P. W. & Calvert, A. T. (2013). Modeling volcano growth on the Island of Hawaii: Deep-water perspectives. *Geosphere* **9**, 1348–1383.

Lofgren, G. (1974). An experimental study of plagioclase crystal morphology: Isothermal crystallization. *American Journal of Science* **274**, 243–244.

Maaløe, S., Pedersen, R. B. & James, D. (1988). Delayed fractionation of basaltic lavas. *Contributions to Mineralogy and Petrology* **98**, 401–407.

Maaløe, S., Tumyr, O. & James, D. (1989). Population density and zoning of olivine phenocrysts in tholeiites from Kauai, Hawaii. *Journal of Petrology* **33**, 761–784.

Macdonald, G. A. (1949). *Petrography of the Island of Hawaii. US Geological Survey, Professional Paper* **214-D**, 96 pp.

Macdonald, G. A. & Katsura, T. (1964). Chemical composition of Hawaiian lavas. *Journal of Petrology* **5**, 82–133.

Marske, J. P., Pietruszka, A. J., Weis, D., Garcia, M. O. & Rhodes, J. M. (2007). Rapid passage of a small-scale mantle heterogeneity through the melting regions of Kilauea and Mauna Loa volcanoes. *Earth and Planetary Science Letters* **259**, 34–50.

Matzen, A. K., Baker, M. B., Beckett, J. R. & Stolper, E. M. (2011). Fe–Mg partitioning between olivine and high-magnesian melts and the nature of Hawaiian parental liquids. *Journal of Petrology* **52**, 1243–1263.

McDonough, W. F. & Sun, S. S. (1995). The composition of the Earth. *Chemical Geology* **120**, 223–253.

McDougall, I. (1964). Potassium–argon ages from lavas of the Hawaiian Islands. *Geological Society of America Bulletin* **75**, 107–128.

McDougall, I. (1979). Age of shield-building volcanism of Kauai and linear migration of volcanism in the Hawaiian island chain. *Earth and Planetary Science Letters* **46**, 31–42.

Montierth, C., Johnston, A. D. & Cashman, K. V. (1995). An empirical glass-composition-based geothermometer for Mauna Loa lavas. In: Rhodes, J. M. & Lockwood, J. P. (eds) *Mauna Loa Revealed. American Geophysical Union, Geophysical Monograph* **92**, 207–217.

Moore, J. G. (1965). Petrology of deep-sea basalts near Hawaii. *American Journal of Science* **263**, 40–52.

Moore, J. G., Normark, W. R. & Holcomb, R. T. (1994). Giant Hawaiian landslides. *Annual Review of Earth and Planetary Sciences* **22**, 119–144.

Mukhopadhyay, S., Lassiter, J. C., Farley, K. A. & Bogue, S. W. (2003). Geochemistry of Kauai shield-stage lavas: Implications for the chemical evolution of the Hawaiian plume. *Geochemistry, Geophysics, Geosystems* **4**(**1**), 1009, doi:10.1029/2002GC000342.

Nakamura, M. (1995). Residence time and crystallization history of nickeliferous olivine phenocrysts from the northern Yatsuga-take volcanoes, Central Japan. *Journal of Volcanology and Geothermal Research* **66**, 81–100.

Niu, Y. L., Collerson, K. D., Batiza, R., Wendt, J. I. & Regelous, M. (1999). Origin of enriched-type mid-ocean ridge basalt at ridges far from mantle plumes: The East Pacific Rise at 11°20′N. *Journal of Geophysical Research* **104**, 7067–7087.

Nobre Silva, I. G., Weis, D., Barling, J. & Scoates, J. S. (2009). Leaching systematics and matrix elimination for the determination of high-precision Pb isotope compositions of ocean island basalts. *Geochemistry, Geophysics, Geosystems* **10**, Q08012, doi:10.1029/2009GC002537.

Nobre Silva, I. G., Weis, D. & Scoates, J. S. (2010). Effects of acid leaching on the Sr–Nd–Hf isotopic compositions of ocean island basalts. *Geochemistry, Geophysics, Geosystems* **11**, Q09011, doi:10.1029/2010gc003176.

Nobre Silva, I. G., Weis, D. & Scoates, J. S. (2013). Isotopic systematics of the early Mauna Kea shield phase and insight into the deep mantle beneath the Pacific Ocean. *Geochemistry, Geophysics, Geosystems* **14**, 659–676.

Norman, M. D. & Garcia, M. O. (1999). Primitive tholeiitic magma compositions and source characteristics of the Hawaiian Plume: Constraints from Picritic Lavas. *Earth Planetary Science Letters* **168**, 19–26.

Ozawa, A., Tagami, T. & Garcia, M. O. (2005). Unspiked K–Ar dating of the Honolulu rejuvenated and Koolau shield volcanism on Oahu, Hawaii. *Earth and Planetary Science Letters* **232**, 1–11.

Pietruszka, A. J., Norman, M. D., Garcia, M. O., Marske, J. & Burns, D. H. (2013). Chemical heterogeneity in the Hawaiian mantle plume from the alteration and dehydration of recycled oceanic crust. *Earth and Planetary Science Letters* **361**, 298–309.

Pretorius, W., Weis, D., Williams, G., Hanano, D., Kieffer, B. & Scoates, J. S. (2006). Complete trace elemental characterisation of granitoid (USGS G-2, GSP-2) reference materials by high resolution inductively coupled plasma-mass spectrometry. *Geostandards and Geoanalytical Research* **30**, 39–54.

Putirka, K. D., Perfit, M. & Ryerson, F. J. (2007). Ambient and excess mantle temperatures, olivine thermometry, and active vs passive upwelling. *Chemical Geology* **241**(**3–4**), 177–206.

Regelous, M., Niu, Y., Wendt, J. I., Batiza, R., Greig, A. & Collerson, K. D. (1999). Variations in the geochemistry of magmatism on the East Pacific Rise at 10°30′N since 800 ka. *Earth and Planetary Science Letters* **168**(**1–2**), 45–63.

Ren, Z. Y., Ingle, S., Takahashi, E., Hirano, N. & Hirata, T. (2005). The chemical structure of the Hawaiian mantle plume. *Nature* **436**, 837–840.

Rhodes, J. M. (1996). Geochemical stratigraphy of lava flows sampled by the Hawaii Scientific Drilling Project. *Journal of Geophysical Research* **101**, 11729–11746.

Rhodes, J. M. & Vollinger, M. J. (2004). Composition of basaltic lavas sampled by phase-2 of the Hawaii Scientific Drilling Project: Geochemical stratigraphy and magma types. *Geochemistry,* Geophysics*, Geosystems* **5**, Q03G13, doi:10.1029/2002GC000434.

Ribe, N. M. & Christensen, U. R. (1999). The dynamical origin of Hawaiian volcanism. *Earth and Planetary Science Letters* **171**, 517–531.

Robinson, J. E. & Eakins, B. W. (2006). Calculated volumes of individual shield volcanoes at the young end of the Hawaiian ridge. *Journal of Volcanology and Geothermal Research* **151**, 309–317.

Sherrod, D. R., Murai, T. & Tagami, T. (2007a). New K–Ar ages for calculating the end-of shield extrusion rates at West Maui volcano, Hawaiian island chain. *Bulletin of Volcanology* **69**, 627–642.

Sherrod, D. R., Sinton, J. M., Watkins, S. E. & Brunt, K. M. (2007b). *Geologic map of the State of Hawaii. US Geological Survey, Open-File Report **2007–1089***, http://pubs.usgs.gov/of/2007/1089/.

Sobolev, A. V., Hofmann, A. W., Sobolev, S. V. & Nikogosian, I. K. (2005). An olivine-free mantle source of Hawaiian shield basalts. *Nature* **434**, 590–597.

Sobolev, A. V., Hofmann, A. W., Kuzmin, D. V., et al. (2007). The amount of recycled crust in source of mantle-derived melts. *Science* **316**, 412–417.

Sun, S.- S. & McDonough, W. F. (1989). Chemical and isotopic systematic of oceanic basalts: implications for mantle composition and processes. In: Saunders, A. D. & Norry, M. J. (eds.), *Magmatism in the Ocean Basins*. Geological Society, London, Special Publications **42**, 313–345.

Takahashi, E., Moore, J. G., Yosoke, H., Clague, D. A., Nakagawa, M., Kani, T., Coombs, M., Moore, G., Harada, Y., Kunikiyo, T. & Robinson, J. (2001). A newly recognized shield volcano southwest of Oahu Island, Hawaii. *EOS Transactions, American Geophysical Union* **82**(**47**), Fall Meeting Supplement, Abstract V12B-0981.

Tanaka, R., Makishima, A. & Nakamura, E. (2008). Hawaiian double volcanic chain triggered by an episodic involvement of recycled material: Constraints from temporal Sr–Nd–Hf–Pb isotopic trend of the Loa-type volcanoes. *Earth and Planetary Science Letters* **265**, 450–465.

Tatsumoto, M. (1978). Isotopic composition of lead in oceanic basalt and its implication to mantle evolution. *Earth and Planetary Science Letters* **38**, 63–87.

Vidal, V. & Bonneville, A. (2004). Variations of the Hawaiian hot spot activity revealed by variations in magma production rate. *Journal of Geophysical Research* **109**, B03104, doi:10.1029/2003JB002559.

Wanless, V. D., Garcia, M. O., Rhodes, J. M., Weis, D., Norman, M., Fornari, D. J., Kurz, M. & Guillou, H. (2006). Submarine radial vents on Mauna Loa Volcano, Hawai`i. *Geochemistry, Geophysics, Geosystems* **7**, Q05001, doi:10.1029/2005GC001086.

Weis, D., Kieffer, B., Maerschalk, C., Pretorius, W. & Barling, J. (2005). High-precision Pb–Sr–Nd–Hf isotopic characterization of USGS BHVO-1 and BHVO-2 reference materials. *Geochemistry, Geophysics, Geosystems* **6**, 2004GC000852.

Weis, D., Kieffer, B., Maerschalk, C., Barling, J., de Jong, J., Williams, G. A., Hanano, D., Pretorius, W., Mattielli, N., Scoates, J. S., Goolaerts, A., Friedman, R. M. & Mahoney, J. J. (2006). High-precision isotopic characterization of USGS reference materials by TIMS and MC-ICP-MS. *Geochemistry, Geophysics, Geosystems* **7**, 2006GC001283.

Weis, D., Kieffer, B., Hanano, D., Nobre Silva, I., Barling, J., Pretorius, W., Maerschalk, C. & Mattielli, N. (2007). Hf isotope compositions of U.S. Geological Survey reference materials. *Geochemistry, Geophysics, Geosystems* **8**, 2006GC001473.

Weis, D., Garcia, M. O., Rhodes, J. M., Jellinek, M. & Scoates, J. S. (2011). Role of the deep mantle in generating the compositional asymmetry of the Hawaiian mantle plume. *Nature Geoscience* **4**, 831–838.

Wessel, P. & Kroenke, L. W. (2007). Reconciling late Neogene Pacific absolute and relative plate motion changes. *Geochemistry, Geophysics, Geosystems* **8**, Q08001, doi:10.1029/2007GC001636.

Xu, G., Huang, S., Frey, F. A., Blichert-Toft, J., Abouchami, W., Clague, D. A., Cousens, B., Moore, J. G. & Beeson, M. H. (2014). The distribution of geochemical heterogeneities in the source of Hawaiian shield lavas as revealed by a transect across the strike of the Loa and Kea spatial trends: East Molokai to West Molokai to Penguin Bank. *Geochimica et Cosmochimica Acta* **132**, 214–237.